Systematics of isospin character of transitions to the 2_1^+ and 3_1^- states in ^{90,92,94,96}Zr

D. J. Horen, R. L. Auble, J. Gomez del Campo, G. R. Satchler, R. L. Varner, and J. R. Beene
Oak Ridge National Laboratory, Oak Ridge, Tennessee 37831

Brian Lund
Department of Physics, Yale University, New Haven, Connecticut 06511

V. R. Brown and P. L. Anthony
Lawrence Livermore National Laboratory, University of California, Livermore, California 94550

V. A. Madsen
Physics Department, Oregon State University, Corvallis, Oregon 97331
(Received 7 October 1992)

Differential cross sections for exciting the 2_1^+ and 3_1^- states of ^{90,92,94,96}Zr with 70-MeV ^{6}Li ions have been measured. Calculations of the cross sections have been performed using a deformed optical model potential (DOMP) with OMP deduced from fits to the elastic data, as well as a folding model with an effective nucleon-nucleon interaction with a Yukawa form factor obtained from fits to the elastic data and transition densities obtained from open-shell random phase approximation (RPA) calculations. The DOMP fits to the data yield values of M_n/M_p which are in good agreement with those predicted using the RPA. For the 2_1^+ states, we find M_n/M_p increases from less than N/Z to greater than N/Z in going from ^{90}Zr to ^{96}Zr. However, for the 3_1^- states M_n/M_p remains less than N/Z for all cases, a result which is in disagreement with previous works. The folding model, with the RPA transition densities, provides good agreement with the 2_1^+ measurements, but underpredicts the cross sections for the 3_1^- states. A reanalysis of the earlier data from excitation of these states by (α,α') reactions removes much of the apparent discrepancies between those measurements and other measurements, including the ones reported here. The localization of the ^{6}Li interaction is also discussed.

PACS number(s): 21.10.Hw, 27.60.+j

I. INTRODUCTION

The experimental determination of the isospin character of nuclear transitions can provide a stringent test of nuclear structure calculations. Most information of this type has been obtained from comparisons of inelastic hadron scattering data with electromagnetic (EM) transition rates deduced from electron scattering, Coulomb excitation, or photon decay. Hadron scattering data are frequently analyzed using the deformed optical model potential (DOMP) [1], and a hadronic deformation length, δ_l^N, is determined from normalization of the calculated to the measured cross sections. The conditions under which these deformation lengths, δ_l^N, extracted from, say, inelastic alpha-particle scattering could be expected to yield meaningful results, when compared with analogous deformation lengths extracted from EM data, were pointed out by Bernstein [2]. Madsen, Brown, and Anderson noted that the deformation length deduced from inelastic scattering is a function not only of the nuclear structure matrix element but of the probe itself [3]. Extensive use has been made of the DOMP in association with a collective vibrational model to analyze inelastic scattering and to map out the isospin character of the transitions to the 2_1^+ and 3_1^- states of even-even nuclei [2,4]. Using data for a variety of probes (protons, alpha particles, neutrons, pions) at a variety of incident energies, the behavior near closed-shell nuclei for the 2_1^+ states was found to be in reasonable agreement with predictions of simple schematic structure models [4,5]. In principle, it is also possible to utilize inelastic scattering by a single probe to deduce the isospin character. This can be accomplished if the experimental parameters can be chosen such that interference between the Coulomb and nuclear amplitudes (CNI) produces structure in the differential cross sections that is sensitive to their relative amplitudes, and, hence, to the isospin character of the transition being measured. This method has been used with heavy-ion projectiles to investigate the isospin character of transitions to both bound states and the giant quadrupole resonance (GQR) [6–9]. The isospin characters determined for the GQR from heavy-ion measurements [6–8] are in conflict with those reported [10,11] from $\pi^\pm$ measurements. However, the results of a recent $\pi^\pm$ measurements [12] for the mixed isospin transition to the 2_1^+ of ^{206}Pb agree well with the heavy-ion [9] data.

The present study was undertaken as an attempt to resolve the large disagreements pertaining to the isospin character for transitions to the 2_1^+ and 3_1^- states in the even zirconium isotopes, as determined from inelastic alpha-particle scattering [13] (CNI technique) and a comparison of inelastic proton and neutron data [14]. The ratio of the neutron multipole transition matrix element, M_n, to the proton multipole transition matrix element,

M_p, reported from alpha scattering [13] is significantly larger ($\geq 50\%$ in most cases) than that from the comparison of neutron and proton scattering [14].

We use the ^{90,92,94,96}Zr(^{6}Li,^{6}Li′) reaction at 70 MeV, and analyze the data using the DOMP, as well as a folding model with an effective nucleon-nucleon interaction [15] in conjunction with transition densities predicted by a quasiparticle random phase approximation (RPA) model with separable isoscalar and isovector particle-hole interactions [16].

We compare our deduced M_n/M_p values with those reported in two previous studies, one which used a comparison of inelastic neutron and proton scattering data and another which used inelastic alpha-particle scattering. We present arguments that can partially resolve several of the large discrepancies that occur between the three works.

We also reanalyze the data from the earlier (α,α') measurements [13], using both DOMP and folding models. We conclude that the published results for the $B(El)$ values obtained from χ^2 fits to the 2_1^+ alpha-scattering data may be somewhat misleading, and that we can reproduce some of these 2_1^+ (α,α') cross sections by DOMP calculations in which we use the same $B(E2)\uparrow$ as are used in the analysis of our ^{6}Li data. Furthermore, when the deduced δ_l^N and these $B(El)\uparrow$ are used to derive M_n/M_p values in a manner consistent with that used with the ^{6}Li data, much better agreement between the two sets of M_n/M_p values is obtained. In addition, we have performed folding model calculations using a standard nucleon-alpha interaction of Gaussian form with our RPA transition densities, and find agreement with the measured 2_1^+ (α,α') cross sections of similar quality to that found for our ^{6}Li data, while the 3_1^- (α,α') cross sections are underpredicted to the same extent as for the ^{6}Li.

II. EXPERIMENT

Measurements of the scattering of 70-MeV ^{6}Li ions by ~ 1.0 mg/cm^2, self-supporting targets of ^{90,92,96,98}Zr were performed utilizing the 25-MV tandem accelerator at the Holifield Heavy-Ion Research Facility (HHIRF) at ORNL. Scattered particles were detected using an Enge, split-pole spectrometer with a two-wire, hybrid particle detector [17], which provided both momentum analysis and particle identification. The overall energy resolution was ~ 225 keV, which was mainly determined by the detector system.

The data were measured over a laboratory angular range $\theta_{\rm lab} \approx 4°-45°$, and analyzed off line in 0.56° bins. A five-slotted plate was inserted in place of the spectrograph slit at each angle setting to calibrate the detector in terms of the scattering angle at the target. For the angles inside $\theta_{\rm lab} = 12°$, this plate was also used to obtain data. The vertical aperture of the defining slits was chosen so that the true scattering angle for trajectories within the bins was essentially equal to the in-plane scattering angle.

The target compositions and thicknesses are given in Table I. In addition to the compositions shown there, some of the targets contained small contaminations of carbon and oxygen (all had been used in previous experiments). The ^{96}Zr target also contained a small amount of tungsten in the ratio of about 0.5% tungsten atoms per atom of zirconium. It was necessary to correct the small-angle ^{96}Zr elastic-scattering data for the tungsten impurity. The main effects of the carbon and oxygen contaminants were on the inelastic spectra at small angles.

TABLE I. Thickness and isotopic composition of the zirconium targets.

Target	Thickness (mg/cm^2)	Abundance (%) ^{90}Zr	^{91}Zr	^{92}Zr	^{94}Zr	^{96}Zr
^{90}Zr	1.035	97.67	0.96	0.71	0.55	0.13
^{92}Zr	0.995	2.86	1.29	94.57	1.15	0.14
^{94}Zr	1.004	1.67	0.42	0.76	96.93	0.22
^{96}Zr	1.006	7.25	1.41	2.24	3.85	85.25

III. MODELS AND ANALYSIS

We have used both "macroscopic" and "microscopic" models to analyze the data. The macroscopic model employs a standard optical model analysis of the elastic scattering and the DOMP. The microscopic model uses a random phase approximation nuclear structure calculation to predict neutron and proton transition densities for use in a folding model calculation of the cross sections. The cross sections were calculated using the computer program PTOLEMY [18].

A. Macroscopic analysis

1. Elastic scattering

The optical model potential was taken to be of the usual Woods-Saxon form,

$$U(r) = -Vf(x_V) - iWf(x_W) , \quad (1)$$

with

$$f(x_i) = (1+e^{x_i})^{-1}, \quad x_i = (r-R_i)/a_i ,$$

$$R_i = r_i(A_p^{1/3} + A_t^{1/3}) \text{ fm} ,$$

and $i = V, W$. The Coulomb potential was taken as that of a point charge interacting with a uniform charge distribution with radius $R_c = r_c(A_p^{1/3} + A_t^{1/3})$ fm, where A_p and A_t are the masses of the projectile and target, respectively. In this work, we adopt a value $r_c = 1.20$ fm.

Absolute elastic cross sections were calculated using the target thickness, experimental geometry, and the Faraday cup readings. Searches were made on the elastic data for each target to determine the optimum optical model parameter values using the computer program PTOLEMY [18]. The usual χ^2 criterion was used when varying the parameter values to produce the optimum fit to the measured cross sections which had relative errors of $\sim 5\%$. A study of the fits to the elastic data implied

that the cross sections for each target should be increased by 12%, and this renormalization was adopted for all the data. As expected, many combinations of optical model parameters could be found that fit the elastic data equally well. These included parameter sets in which the real and imaginary geometries were the same, as well as those in which the two geometries were different.

The OMP parametrizations used in the present work for each isotope are given in Table II. These were used in all of the DOMP calculations pertaining to the ^{6}Li data to be described below. Fits to the elastic data corresponding to the parameters listed in Table II are shown in Fig. 1.

2. *Inelastic scattering*

In the DOMP [1] calculations, the nuclear transition potential for angular momentum transfer l is assumed to be [18]

$$H_l^N(r) = -\delta_V^N(l)\frac{dV(r)}{dr} - i\delta_W^N(l)\frac{dW(r)}{dr} , \quad (2)$$

where $V(r)$ and $W(r)$ are the real and imaginary parts of the optical potential (1) with the parameters taken from the optical model fits to the elastic data. Here, the real and imaginary deformation lengths are assumed to be equal [i.e., $\delta_V^N(l) = \delta_W^N(l) = \delta_l^N$]. To this is added the Coulomb interaction, which at large radii is determined uniquely by the reduced electric transition probability, $B(El)\uparrow$. For radii less than R_c, we used the form for a point charge interacting with a deformed, uniformly charged, sphere of radius R_c, namely,

$$H_l^c(r) = \frac{4Z_p e}{2l+1}[B(El)\uparrow]^{1/2} r^l / R_c^{2l+1} , \quad (3)$$

where Z_p is the atomic number of the projectile. The reduced electric transition probability is given in terms of the proton multipole transition matrix element, M_p, as

$$B(El)\uparrow = e^2 M_p^2 = e^2 \left| \int g_l^p(r) r^{l+2} dr \right|^2 , \quad (4)$$

where $g_l^p(r)$ is the proton transition density, and M_p is the proton 2^l pole moment. The neutron multipole transition matrix element, M_n, is similar to M_p with $g_l^p(r)$ replaced by $g_l^n(r)$ [1].

A mass (or isoscalar) multipole transition matrix element can then be defined as $M_{IS} = M_n + M_p$, which then gives a reduced mass transition probability in analogy to

TABLE II. Optical model parameters determined from least-squares fits to the elastic-scattering data for the ^{90,92,94,96}Zr(^{6}Li,^{6}Li) reaction at $E = 70$ MeV. A Coulomb radius of $r_c = 1.20$ fm was fixed in all cases.

Isotope	V (MeV)	r (fm)	a (fm)	W (MeV)	r_I (fm)	a (fm)
^{90}Zr	61.47	1.020	0.825	188.55	0.870	0.826
^{92}Zr	53.871	1.020	0.854	178.06	0.870	0.843
^{94}Zr	49.846	1.020	0.883	190.09	0.870	0.840
^{96}Zr	49.847	1.019	0.875	59.927	1.019	0.875

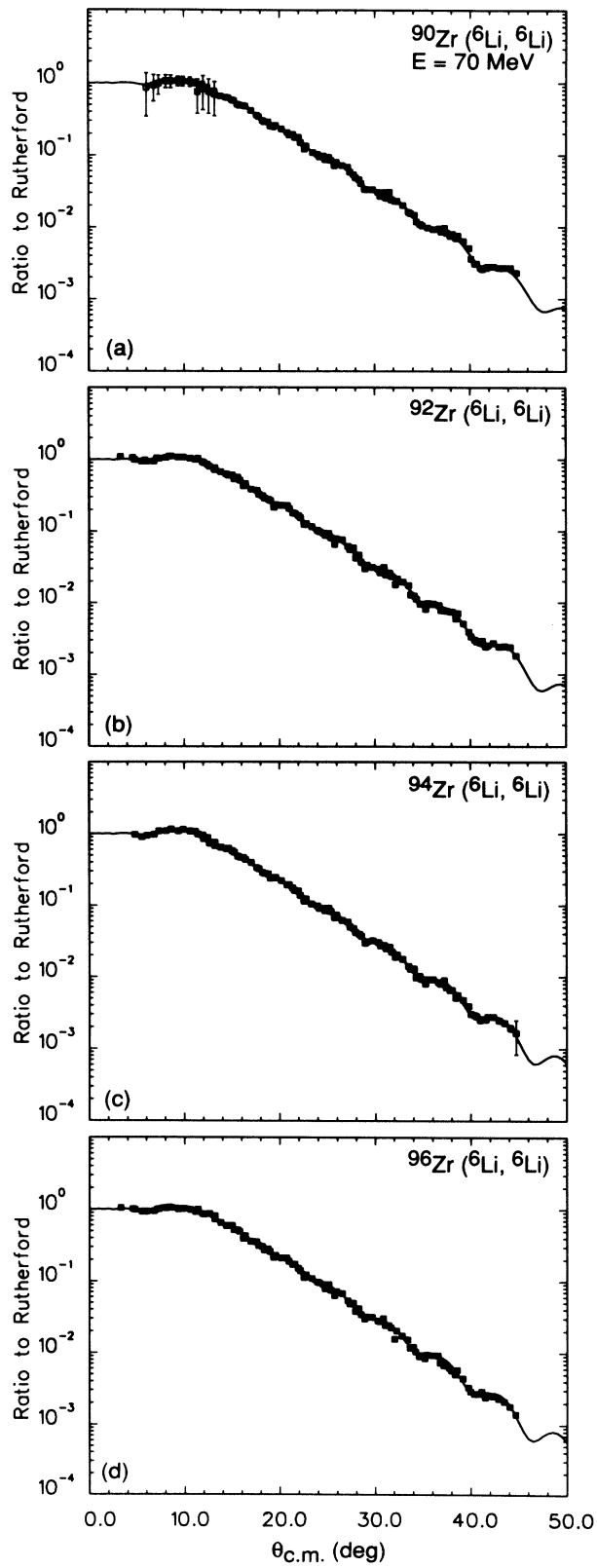

FIG. 1. Optical model fits to the elastic-scattering data for ^{90,92,94,96}Zr+^{6}Li at $E = 70$ MeV. The optical model parameters are given in Table II. The cross-section data are plotted relative to the Rutherford cross section.

that for the charge probability as

$$B_{\rm IS}(l)\uparrow = |M_n + M_p|^2 \ . \tag{5}$$

One can then derive the ratio

$$|M_n/M_p| = \left| \frac{B_{\rm IS}(l)\uparrow}{B(El)\uparrow/e^2} \right|^{1/2} - 1 \ . \tag{6}$$

The ratio M_n/M_p is an indication of the isospin character of the nuclear transition.

We make the usual assumption that the neutron and proton transition densities, $g_l^n(r)$ and $g_l^p(r)$, have the same radial geometry, i.e.,

$$g_l^n(r) = N\delta_l^n g(r), \quad g_l^p(r) = Z\delta_l^p g(r) \ . \tag{7a}$$

Then we may define an isoscalar (or mass) deformation length by

$$\delta_l^{\rm IS} = (N\delta_l^n + Z\delta_l^p)/A \ . \tag{7b}$$

These relations would be obeyed, for example, if the excitations arose from harmonic vibrations of the ground-state densities, and the neutron and proton radial distributions had the same shape. Furthermore, we make the additional assumption that the potential deformation length in the DOMP model (2) is the same as the mass deformation length given in (7b), i.e.,

$$\delta_l^N = \delta_l^{\rm IS} \ , \tag{7c}$$

since the projectile here is an isoscalar probe. A measure of the proton deformation length can be obtained from the $B(El)$ value by using the expressions for a uniform distribution,

$$B(El)\uparrow = (\delta_l^p)^2 \left[\frac{3ZeR_c^{l-1}}{4\pi} \right]^2 , \tag{8}$$

where we choose $R_c = 1.20 A_t^{1/3}$ fm. (This expression corresponds to the proton radial transition density being a delta function at $r = R_c$, but calculations with more realistic shapes indicate that the error made with this assumption is small.)

In the DOMP calculations the magnitude and shape of the differential cross section are functions of the Coulomb and nuclear amplitudes and their relative phases. The calculated cross sections are completely determined by δ_l^p [or $B(El)\uparrow$] and δ_l^N within our model. When the $B(El)\uparrow$ is fairly well known from other works, we fix that value and search on δ_l^N.

The ratio M_n/M_p can now be calculated from the deduced quantities (δ_l^N, δ_l^p) by using Eqs. (6)–(8), i.e.,

$$M_n/M_p = (A\delta_l^N/Z\delta_l^p) - 1 \ . \tag{9}$$

A simple "isoscalar" mass vibration would have $\delta_l^{\rm IS} = \delta_l^n = \delta_l^p$, and consequently $M_n/M_p = N/Z$.

The inelastic cross sections were computed using coupled channels [18]. It was determined that the effects of the inelastic couplings on the elastic scattering were small, so that the optical model parameters deduced from the elastic fits (i.e., Table II) were adequate for use in the calculations of the inelastic cross sections. Calculations

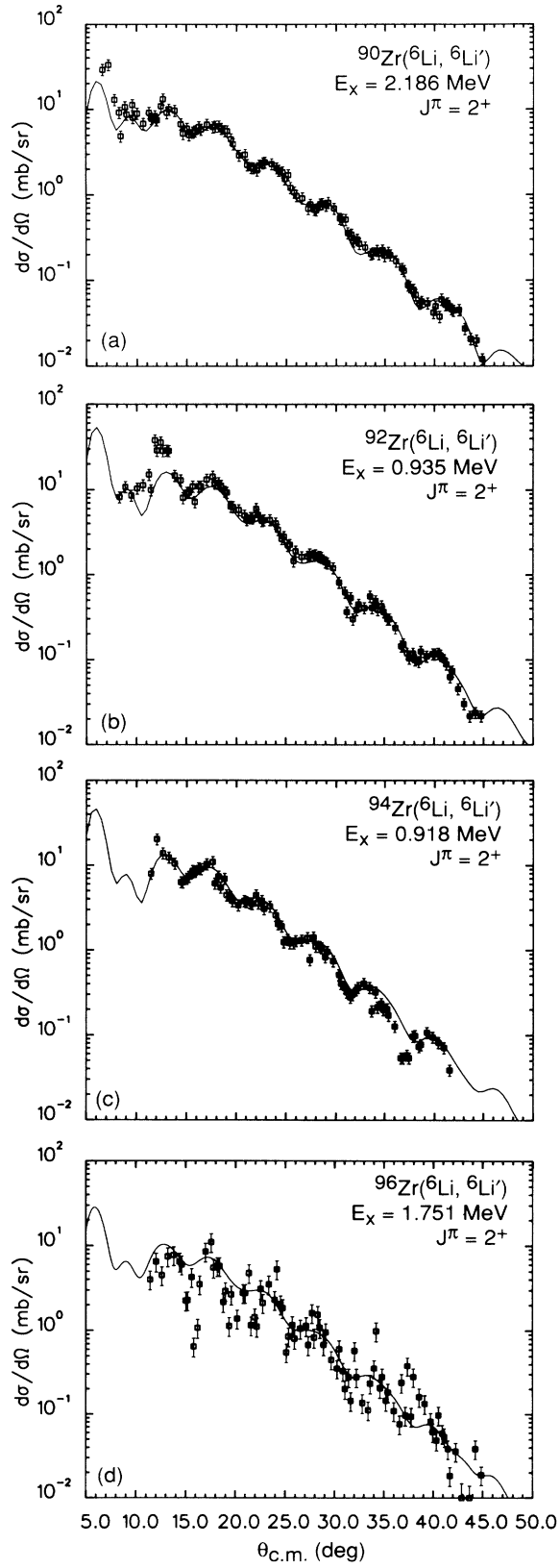

FIG. 2. Differential cross sections for exciting the 2_1^+ states of ^{90,92,94,96}Zr with 70-MeV ^{6}Li ions. The solid curves represent coupled-channels cross sections calculated using the DOMP and the program PTOLEMY.

using other sets of optical model parameters obtained from fits to the elastic data gave essentially identical inelastic cross sections.

a. 2_1^+ *states.* The $B(E2)\uparrow$ values for ^{90}Zr and ^{92}Zr have been fairly well established. For ^{90}Zr, there is excellent agreement between the values determined from measurements of inelastic electron scattering and resonance fluorescence. Only one Coulomb excitation measurement has been reported [19] with a $B(E2)\uparrow$ whose mean value is about $\frac{2}{3}$ of the adopted [20] $B(E2)\uparrow=0.063\pm0.005$ $e^2\,\mathrm{b}^2$. There are three Coulomb excitation measurements of $B(E2)\uparrow$ for ^{92}Zr which are in good agreement, and we utilize the adopted value [20] $B(E2)\uparrow=0.083\pm0.06$ $e^2\,\mathrm{b}^2$. For ^{94}Zr there are two Coulomb excitation values, $B(E2)\uparrow=0.056\pm0.014$ $e^2\,\mathrm{b}^2$ [21] and $0.081\pm0.017 e^2\,b^2$ [22]. In the PTOLEMY calculations we used the adopted value [20] of 0.066 ± 0.014 $e^2\,\mathrm{b}^2$. From a Coulomb excitation measurement on ^{96}Zr, Gangrskii and Lemberg [19] report $B(E2)\uparrow=0.055\pm0.022$ $e^2\,\mathrm{b}^2$. However, as noted above, for ^{90}Zr these authors [19] give $B(E2)\uparrow=0.042\pm0.015$ $e^2\,\mathrm{b}^2$, which is about 30% below the adopted value given above for this transition.

In the DOMP calculations, we fixed the $B(E2)\uparrow$ (i.e., δ_l^p) and varied δ_l^N that we used in the program PTOLEMY. Since PTOLEMY does not have a search routine for inelastic scattering, we performed a series of calculations in which we changed M_n/M_p, by varying δ_l^N in accordance with Eq. (9).

Our final calculations for the 2_1^+ cross sections are shown in Fig. 2, and the deduced M_n/M_p are listed in Table III. For $\theta_{\mathrm{c.m.}}<15°$, the carbon and oxygen contaminants and the tail of the elastic peak affect the accuracy of the deduced cross sections. The discrepancy between the data and calculated cross section near $\theta_{\mathrm{c.m.}}=13°$ for ^{92}Zr [Fig. 2(b)] is caused by the carbon and oxygen contaminants. Unfortunately, it is in that angular region that the signature of the CNI is most pronounced. However, as can be seen in Fig. 3, where we plot the Coulomb and nuclear cross sections separately for exciting the 2_1^+ state in ^{92}Zr, the Coulomb contribution to the total cross section is still significant beyond 15°. Hence, we have searched on the data for ^{90,92}Zr using the computer code ECIS [23] in which we allowed both δ_l^p and δ_l^N to vary simultaneously. From these ECIS fits, we obtained $B(E2)\uparrow=0.066\pm0.06$ $e^2\,\mathrm{b}^2$ and $M_n/M_p=0.72\pm0.10$ for ^{90}Zr, and $B(E2)\uparrow=0.089\pm0.009$ and $M_n/M_p=1.21\pm0.12$ for ^{92}Zr. These $B(E2)\uparrow$ are in good agreement with the adopted values, and the M_n/M_p also agree well with our ratios listed in Table III.

For the 2_1^+ state in ^{94}Zr, a search with ECIS gave $B(E2)\uparrow=0.079\pm0.009$ $e^2\,\mathrm{b}^2$ and $M_n/M_p=1.13\pm0.20$ with a χ^2 within a factor of 2 of that obtained with the adopted $B(E2)\uparrow=0.066$ $e^2\,\mathrm{b}^2$ and $M_n/M_p=1.50\pm0.15$. This points out the need for independent determinations of $B(E2)\uparrow$ and high-quality inelastic data. Our data for ^{96}Zr are too imprecise for utilizing search routines. Our energy resolution of $\sim$225 keV was not sufficient to completely resolve the 2_1^+ (1.75 MeV) and 3_1^- (1.90 MeV) states. Since the excitation of the 3^- state dominates, the decomposition of the spectra resulted in the large angle-to-angle fluctuations in the 2_1^+ cross section as seen in Fig. 2(d).

b. 3_1^- *states.* The region of strong Coulomb nuclear interference in the cross sections exciting the 3_1^- states occurs in the region $\theta_{\mathrm{c.m.}}<15°$. The sensitivity of the shape of the cross sections to combinations of $B(E3)\uparrow$

TABLE III. Comparisons of $B(El)\uparrow$ and M_n/M_p for the first 2^+ and 3^- states in ^{90,92,94,96}Zr.

				Experiment			RPA calculation[a]			
Isotope	J^π	E_x (MeV)	$B(El)\uparrow$ ($e^2\,\mathrm{b}^l$)	M_n/M_p[b]	M_n/M_p[c]	M_n/M_p[d]	E_x (MeV)	M_p ($e\,\mathrm{fm}^l$)	M_n/M_p	N/Z
90	2^+	2.186	0.063[e]	0.85±0.10	0.85±0.06	1.22±0.12	2.51	25.1	0.84	1.25
	3^-	2.748	0.071[f]	0.60±0.08	0.92±0.13	1.80±0.31	2.73	267	0.75	
92	2^+	0.935	0.083[e]	1.30±0.10	1.05±0.07	2.91±0.19	1.40	28.9	1.49	1.30
	3^-	2.340	0.067[g]	0.85±0.10	1.20±0.13	2.52[j]±0.45	2.64	257	0.87	
94	2^+	0.918	0.066[e]	1.50±0.15	1.50±0.22	3.02±0.22	1.55	25.9	1.69	1.35
	3^-	2.057	0.087[g]	0.90±0.10	1.95±0.20[h]	2.36±0.51	2.35	295	1.06	
96	2^+	1.75	0.055[e]	1.50±0.15		4.62[k]±0.64	2.02	23.3	1.66	1.4
	3^-	1.90	0.12[i]	1.10±0.10		2.67±0.47	1.96	346	1.22	

[a]The interaction strengths were adjusted to reproduce the $B(El)\uparrow$ values quoted in column 4.
[b]This work. The uncertainties do not include uncertainties in the $B(El)\uparrow$.
[c]Reference [14].
[d]Reference [13].
[e]Reference [20].
[f]Reference [24].
[g]Reference [25].
[h]We believe the value 1.59±0.20 given in Ref. [14] is a misprint, based upon our recalculation of this quantity.
[i]We use the value of $B(E3)\uparrow$ from fits to our data which give the largest M_n/M_p.
[j]We believe the value 2.17 given in Ref. [13] is a misprint, based upon our recalculation of this quantity.
[k]We believe the value 4.69 given in Ref. [13] is a misprint, based upon our recalculation of this quantity.

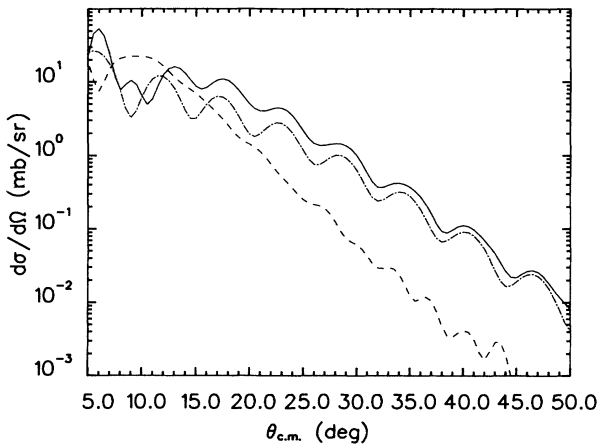

FIG. 3. Calculations of the differential cross sections for exciting the 2_1^+ state of ^{92}Zr at 0.935 MeV using the DOMP and the program PTOLEMY. The dashed curve corresponds to the cross section arising from Coulomb excitation only, the dot-dashed curve to nuclear only, and the solid curve to the total cross section.

and M_n/M_p is rather poor. This means that it would be extremely difficult to independently deduce $B(E3)\uparrow$ from the data. Hence, we rely on other measurements of $B(E3)\uparrow$ to deduce M_n/M_p from our data. Unfortunately, the status of our knowledge of the $B(E3)\uparrow$ for the zirconium isotopes is rather poor. There are no $B(E3)\uparrow$ determined from Coulomb excitation measurements for $^{90-96}$Zr. For ^{90}Zr, we adopt a recent value [24] from (e,e') scattering of $B(E3)\uparrow=0.071\pm0.003$ e^2b^3. For ^{92,94}Zr, we adopt the values $B(E3)\uparrow=0.067$ and 0.087 e^2b^3, respectively [25]. These are based upon DOMP analyses of inelastic proton measurements, and must be considered as indirect and approximate values. In addition to an adopted [25] $B(E3)\uparrow=0.183$ e^2b^3 for ^{96}Zr which is also based upon inelastic proton scattering, there are two recent values obtained from lifetime measurements, i.e., $B(E3)\uparrow=0.25\pm0.04$ e^2b^3 [26] and $0.265^{+0.129}_{-0.067}$ [27]. These latter values would represent one of the strongest $E3$ transitions observed thus far.

Our cross sections for the 3^- excitations calculated using PTOLEMY are shown in Fig. 4 and our deduced M_n/M_p are given in Table III. To reproduce our data for the 3^- state in ^{96}Zr would require M_n/M_p considerably less than 0.9 if we use $B(E3)\uparrow=0.18$ e^2b^3, and less than 0.5 if we use the larger values reported from the lifetime measurements. The CNI signature is not sufficient to search independently on both δ_l^N and δ_l^p in order to deduce a unique value of $B(E3)\uparrow$. Hence, a broad range of δ_l^N and δ_l^p can reproduce the data with comparable χ^2. For ^{96}Zr, the results shown correspond to $B(E3)\uparrow=0.12$ e^2b^3. This value was adopted because it gives the maximum M_n/M_p of 1.10 which is consistent with our cross sections. Should the larger values [26,27] of $B(E3)\uparrow$ prove correct, this would necessitate a revised analysis of the data.

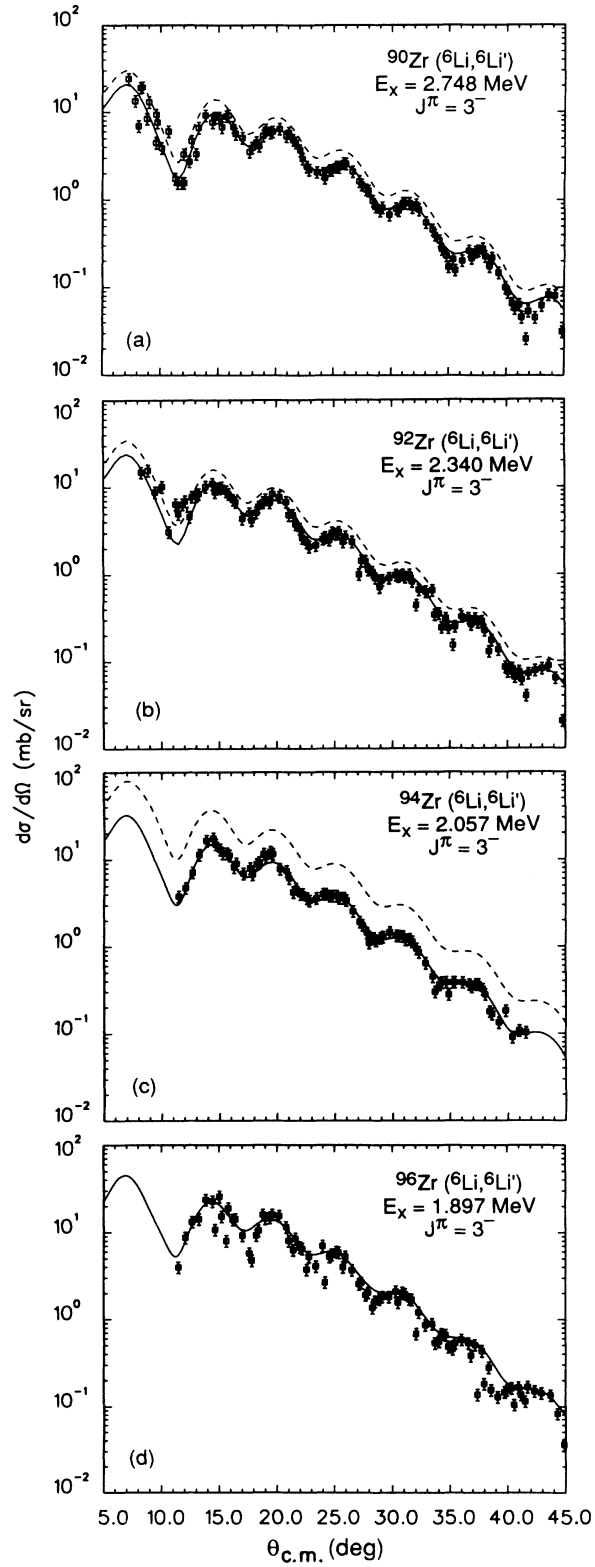

FIG. 4. Comparison of coupled-channels calculations using the DOMP and the program PTOLEMY with the differential cross sections for exciting the 3_1^- states of ^{90,92,94,96}Zr with 70-MeV ^{6}Li ions. The solid curves are for M_n/M_p values determined in this work, and the dashed curves use M_n/M_p reported in Ref. [14].

B. Microscopic analysis

In this section, we discuss the use of a simple nucleon-nucleon interaction that has been found to fit our elastic data, and subsequent folding model calculations of inelastic cross sections. In addition, we examine the radial region of the transition density sampled in the interaction by performing folding calculations assuming an isoscalar Tassie form.

1. Elastic scattering

Folded potentials were used to analyze the elastic data, in order to be consistent with the use of folded transition potentials to describe the inelastic scattering. The optical potential is obtained by the folding of an effective (complex) nucleon-nucleon interaction, $v(r_{12})$, with the projectile and target density distributions [1], i.e.,

$$U_F(r)=\int\int \rho_A(r_1)\rho_{\mathrm{Li}}(r_2)v(r_{12})d\mathbf{r}_1 d\mathbf{r}_2 , \quad (10)$$

where $r_{12}=|\mathbf{r}+\mathbf{r}_2-\mathbf{r}_1|$. For our purpose, it was assumed that the real and imaginary parts of $v(r_{12})$ have the same shape.

The density distribution for ^{6}Li was chosen to be one previously used [28], constructed from the shell model, while two-parameter Fermi shapes were used for the zirconium densities with parameters (Table IV) derived from a systematic study [29]. The results were found to be insensitive to small changes in the latter parameters.

An interaction called the M3Y is frequently used [28] for $v(r_{12})$, but was found to be inadequate (even with renormalization) to describe the present data. On the other hand, previous studies [15] of ^{16,17}O scattering from several targets over a range of energies showed that a simple Yukawa form with a range of $t=0.7$ fm gave good results,

$$v(r)=-(v+iw)\exp(-r_{12}/t)/(r_{12}/t) . \quad (11)$$

The strengths v,w were found to be slowly dependent on energy, with

$$v\approx 54-0.22E(\mathrm{MeV})/A \ \mathrm{MeV} . \quad (12)$$

A similar interaction was tried in the present case. By gridding on the value of t and varying v and w for the best fit at each t, it was confirmed that the optimum range was close to $t=0.7$ fm for each zirconium isotope.

Consequently, we fixed $t=0.7$ fm and obtained the optimum v and w values for each isotope which are listed in Table V. They are consistently $v\approx w\approx 55$ MeV, which are a few percent larger than the values [15] obtained from the ^{16,17}O scattering. The agreement obtained with these two-parameter fits, and the associated χ^2 values, are very similar to those found using Woods-Saxon potentials. The fits to the elastic data using the folding calculations are shown in Fig. 5.

TABLE IV. Parameter values for a two-parameter Fermi model of the ground-state densities of the zirconium isotopes, deduced from Ref. [29], where $\rho(r)=\rho_0(1+e^{(r-c)/a})^{-1}$ and R is the rms radius.

A	c (fm)	a (fm)	R (fm)
90	5.033	0.475	4.280
92	5.076	0.475	4.311
94	5.119	0.475	4.341
96	5.162	0.475	4.372

TABLE V. Strengths of the real and imaginary parts of the effective nucleon-nucleon interaction with Yukawa form and a range of 0.7 fm, which fit the elastic ^{6}Li scattering from the zirconium isotopes.

A	v (MeV)	w (MeV)
90	54.01	56.68
92	53.82	54.05
94	56.42	55.88
96	55.08	54.17

2. Inelastic scattering

The transition potentials were calculated with a computer program which uses fast Fourier transforms to evaluate the generalization of Eq. (10) in which the target ground-state density is replaced by the transition densities [28]. In this paper, the results of using transition densities obtained from quasiparticle random phase approximation calculations [16] are reported. (The use of other forms will be discussed elsewhere [30].) These transition potentials were used in the program PTOLEMY [18] to calculate the inelastic scattering, using as diagonal potentials the corresponding folded potentials fitted to the elastic data. The Yukawa strengths v and w are those given in Table V.

a. RPA model transition densities. The ratio M_n/M_p and the transition densities were determined from a quasiparticle random phase approximation with simple separable quadrupole or octupole interactions with a ratio [4] of unlike ($v_{np}=v_{pn}$) to like ($v_{nn}=v_{pp}$) interactions of 3/1. Harmonic-oscillator (HO) wave functions were used as a basis to describe both the neutron and proton single-particle states. The oscillator parameters which were chosen resulted in rms radii for the ground-state densities which agree within 1% with the values given in Table IV. All single-particle levels from major HO shells $N=0$ to 7 (as well as $N=l=8$, $k=\frac{17}{2}$) were included. For the $N=4$ major neutron shell (including the $h=\frac{11}{2}$ orbital), the single-particle energies where changed from the values given by the Nilsson formula to those given by Kisslinger and Sorensen (KS) [31]. The reason for this substitution is to reproduce the experimental level ordering for the zirconium isotopes which has the $3s_{1/2}$ orbit following the $2d_{5/2}$, and the $1g_{7/2}$ orbit raised above the $1h_{11/2}$ [32]. The KS level spacings were used in the calculations for ^{90}Zr, and were slightly compressed for the other isotopes to avoid giving false systematic differences in their shell gaps. The proton single-particle energies were taken from the Nilsson formula except for the $2p_{3/2}$ level in the $N=3$ filling shell which was adjusted slightly

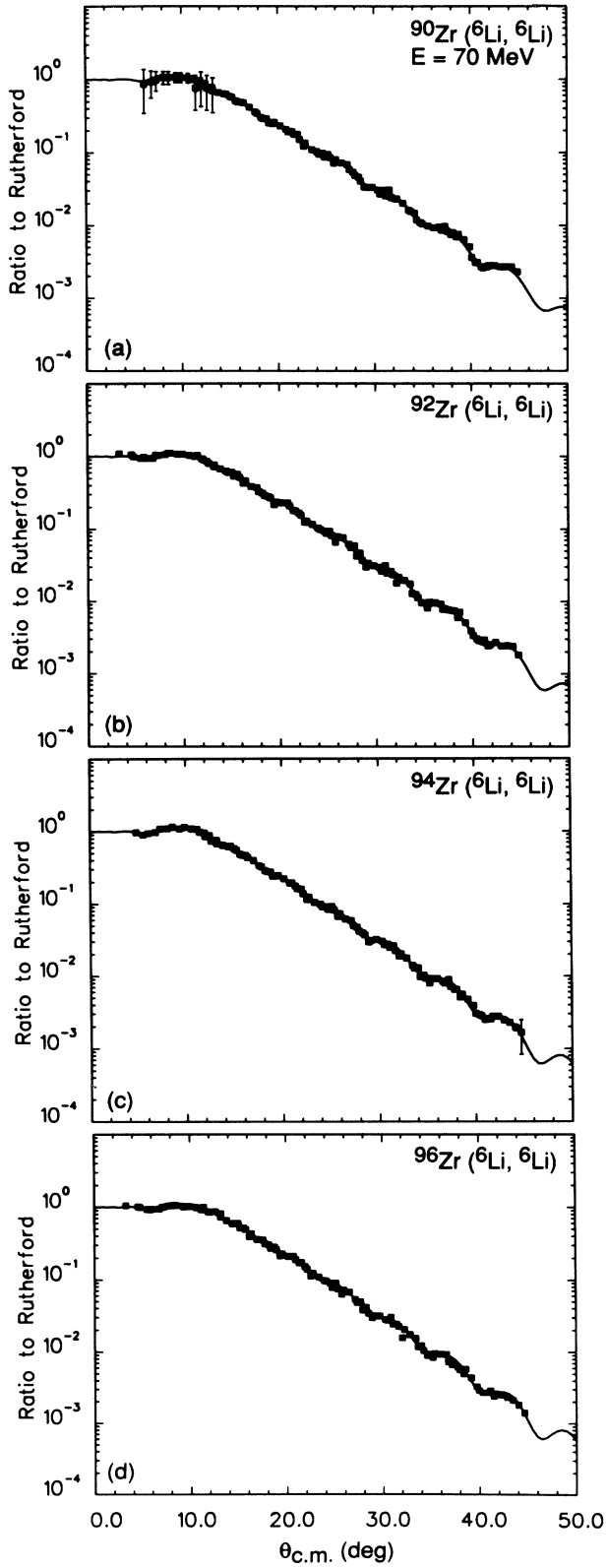

FIG. 5. Folding model fits to the elastic-scattering data for ^{90,92,94,96}Zr+^{6}Li at $E=70$ MeV using an effective nucleon-nucleon interaction. The cross sections are plotted relative to the Rutherford cross sections. The strengths of the interaction are given in Table V.

to reproduce the inner lobes of the experimental transition densities [33] for ^{90}Zr and ^{88}Sr.

The strengths of the quadrupole-quadrupole and octupole-octupole interactions were adjusted separately for each isotope to give approximately the experimental $B(El)\uparrow$ values. This procedure typically gives too high an energy for the quadrupole states, but is considered to be preferable to fitting the energies which would be expected to be lowered by two-particle–two-hole configurations which are neglected in the RPA. On the other hand, two-particle–two-hole configurations would not be expected to contribute substantially to the $B(El)\uparrow$, which is determined by matrix elements of a one-body operator. An alternative procedure in which we attempted to use a one-parameter interaction strength which varied smoothly with A, failed to reproduce the experimental $B(E\lambda)$ systematics.

The resulting neutron and proton transition densities for the 2_1^+ and 3_1^- states are shown in Figs. 6 and 7, respectively. A distinctive feature for the 2_1^+ in ^{92,94,96}Zr is the large inner peak of the neutron transition density near $r=2.5$ fm. This arises mainly because of contributions which involve the $2d_{5/2}$ orbit, which are not present for ^{90}Zr.

In Table VI we list some of the strongest one-particle–one-hole (1p-1h) contributions to M_n and M_p of both valence and core type. The *valence* space is defined to include only single-particle levels in the last filling shell. For the zirconium isotopes, this is the $N=4$ major shell for neutrons ($d_{5/2},s_{1/2},h_{11/2},d_{3/2},g_{7/2}$) and $N=3$ major shell for protons ($p_{3/2},f_{5/2},p_{1/2},g_{9/2}$). All other single-particle levels constitute the core space. *Valence transitions* are defined as those that take place between single-particle states that lie within the valence space, while "core" transitions occur between "core" states as well as those that involve both valence and "core" states. The validity of the core polarization concept for the 2_1^+ states can be readily observed in Table VI. The valence structure of the neutrons is changing as one goes from ^{90}Zr to ^{96}Zr. Because of the strong interaction between unlike nucleons, this change affects most strongly the core protons. For example, as we go from ^{90}Zr with no valence neutrons to ^{92,94,96}Zr, there is a sudden rise of proton core strength, as exhibited, e.g., by the $1f_{7/2}$-$1h_{11/2}$ p-h transition, which roughly tracks with the $2d_{5/2}$-$2d_{5/2}$ neutron valence strength in ^{92,94,96}Zr. The same behavior is observed in the other core-polarization contributions. For the 3_1^- states, the transitions are much less dominated by the valence components, so the core polarization, treated as a perturbation on the valence behavior, is a less appropriate description. The predicted M_n/M_p ratios and excitation energies are compared with the experimental values in Table III.

The RPA proton transition densities for the 2_1^+ and 3_1^- states of ^{90}Zr are compared to those deduced from inelastic electron scattering [34] in Fig. 8. The RPA transition densities reproduce the shapes of those deduced from inelastic electron scattering reasonably well, although the positions of the main lobes occur at slightly smaller radii and the widths are somewhat broader.

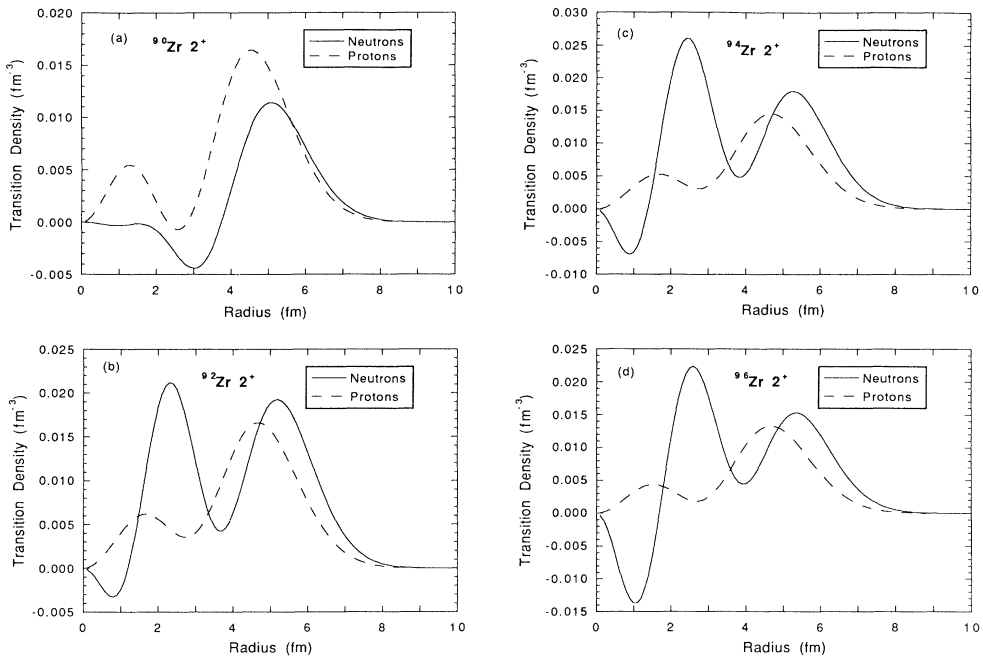

FIG. 6. Neutron and proton transition densities for exciting the 2_1^+ states of ^{90,92,94,96}Zr predicted by the RPA calculations.

b. 2_1^+ *states.* The results of the folding model calculations of the cross sections for exciting the 2_1^+ states using the RPA transition densities are shown in Fig. 9. Overall, the agreement between the predicted and measured cross sections is considered good.

c. 3_1^- *states.* The folding model calculations for the 3_1^- states are compared with the data in Fig. 10, where it is seen that the model consistently underpredicts the cross sections. The underlying reason for this is not yet understood, and it is not clear whether the problem lies with our rather simple interaction or with the ingredients of the RPA.

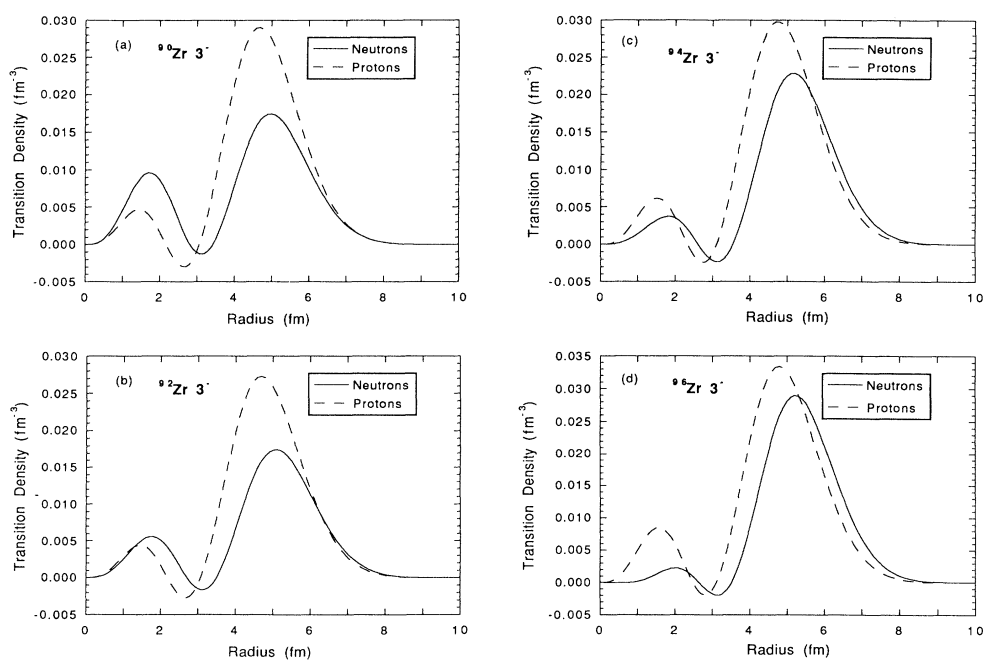

FIG. 7. Neutron and proton transition densities for exciting the 3_1^- states of ^{90,92,94,96}Zr predicted by the RPA calculations.

C. Investigation of the radial localization of the inelastic interaction: Dependence of the inelastic cross section on a radial cutoff of the transition density

It is sometimes speculated that only the extreme tail of the transition density is active in inducing excitation of nuclear states by inelastic scattering because of the strong absorption of the projectile which is experienced in closer encounters. One way to test this hypotheses is to perform a series of calculations using transition densities which have been set to zero for radii less than a cutoff value, RCUT. By studying the variation of the calculated cross section, we obtain some measure of which radial region of the transition density is contributing significantly.

Here we investigate the effects on the inelastic cross section of cutting off the transition density inside a radius, RCUT, for the 3^- transition in ^{94}Zr. We utilize the effective nucleon-nucleon Yukawa interaction described earlier, and a Tassie form factor for the transition density. We assume that the protons and neutrons have identical form factors, and that the transition is "isoscalar." Similar results are attained with a transition density of Bohr-Mottelson shape, which peaks at a slightly smaller radius.

In Fig. 11(a), the transition density is plotted as a function of radius, and the different cutoff radii are indicated. These correspond to RCUT=0, 4, 5, 5.5, 7, 8.5, and 10 fm. The transition density is set to zero for $r<$RCUT. In the folding calculations, the transition density extended out to 16 fm.

The computer code used for calculating the transition potentials uses a fast Fourier transform. To ensure that the sharp cutoff did not introduce spurious numerical effects, we performed a Fourier transform followed by an inverse Fourier transform to see how the resulting transition density compared with the original one. In all cases, it was essentially identical with the input one.

The corresponding transition potentials are shown in

TABLE VI. Partial listing of contributions to the neutron and proton multiple matrix elements, M_n and M_p (in units of fm^l), from the RPA calculations for excitations of the 2_1^+ and 3_1^- states in ^{90,92,94,96}Zr.

	Neutrons					Protons			
1h-1p	^{90}Zr	^{92}Zr	^{94}Zr	^{96}Zr	1h-1p	^{90}Zr	^{92}Zr	^{94}Zr	^{96}Zr
				2_1^+ state					
$2d_{5/2}$-$2d_{5/2}$		11.50	12.36	7.45	$1g_{9/2}$-$1g_{9/2}$	4.75	3.55	3.38	3.9
$1g_{9/2}$-$1i_{13/2}$	4.33	6.35	5.43	4.40	$2p_{3/2}$-$2p_{1/2}$	7.74	2.96	2.88	3.86
$1g_{9/2}$-$2d_{5/2}$	7.58	5.25	2.88	1.32	$1f_{7/2}$-$1h_{11/2}$	2.31	4.67	4.27	3.49
$1f_{7/2}$-$1h_{11/2}$	2.39	3.50	2.96	2.34	$1f_{5/2}$-$2p_{1/2}$	2.15	2.06	1.89	1.86
$2d_{5/2}$-$3s_{1/2}$		3.29	6.15	10.15	$1f_{5/2}$-$1h_{9/2}$	1.40	2.87	2.63	2.15
$1f_{5/2}$-$1h_{9/2}$	1.61	2.40	2.05	1.66	$1d_{5/2}$-$1g_{9/2}$	1.03	2.11	1.95	1.60
$2p_{3/2}$-$2f_{7/2}$	0.74	1.11	0.94	0.76	$2p_{3/2}$-$2p_{3/2}$	0.41	0.43	0.36	0.31
$1d_{3/2}$-$1g_{7/2}$	0.64	0.96	0.81	0.64	$2p_{3/2}$-$2f_{7/2}$	0.70	1.44	1.33	1.09
$2d_{5/2}$-$2g_{9/2}$		0.69	1.15	1.29	$1d_{3/2}$-$1g_{7/2}$	0.70	1.42	1.30	1.06
$1h_{11/2}$-$1h_{11/2}$		0.33	0.65	1.19	$1g_{9/2}$-$2d_{5/2}$	0.47	0.80	0.67	0.50
$2p_{1/2}$-$2f_{5/2}$	0.37	0.56	0.48	0.39	$1f_{5/2}$-$1f_{5/2}$	0.23	0.31	0.26	0.19
$2d_{5/2}$-$2d_{3/2}$		0.44	0.77	0.98	$1g_{9/2}$-$1i_{13/2}$	0.42	0.79	0.65	0.47
$1g_{9/2}$-$1g_{7/2}$	0.30	0.40	0.34	0.28	$2p_{1/2}$-$2f_{5/2}$	0.25	0.53	0.49	0.42
$1g_{7/2}$-$1g_{7/2}$		0.14	0.26	0.47	$2s_{1/2}$-$2d_{5/2}$	0.22	0.44	0.40	0.33
$1g_{7/2}$-$2d_{5/2}$		0.21	0.37	0.50	$1f_{7/2}$-$2p_{3/2}$	0.20	0.33	0.26	0.19
$2d_{3/2}$-$3s_{1/2}$		0.18	0.36	0.72	$1f_{7/2}$-$2f_{7/2}$	0.16	0.32	0.29	0.24
$1g_{7/2}$-$2d_{3/2}$		0.14	0.25	0.44	$2p_{3/2}$-$1f_{5/2}$	0.13	0.20	0.17	0.14
				3_1^- state					
$2d_{5/2}$-$1h_{11/2}$		41.15	89.56	129.93	$2p_{3/2}$-$1g_{9/2}$	123.35	120.27	113.80	111.76
$1g_{9/2}$-$1h_{11/2}$	39.52	33.07	37.09	42.58	$1f_{7/2}$-$1g_{9/2}$	16.34	15.80	20.66	26.42
$1g_{9/2}$-$1j_{15/2}$	25.97	22.53	26.69	32.58	$1f_{7/2}$-$1i_{13/2}$	12.67	12.20	16.35	21.58
$1f_{7/2}$-$1i_{13/2}$	13.42	11.76	13.93	16.97	$2p_{1/2}$-$1g_{7/2}$	8.89	8.78	11.71	15.45
$2p_{1/2}$-$1g_{7/2}$	9.66	8.26	9.49	11.14	$1f_{5/2}$-$1g_{7/2}$	9.02	8.71	11.46	14.85
$1f_{5/2}$-$1i_{11/2}$	9.05	7.92	9.40	11.48	$2p_{1/2}$-$2d_{5/2}$	8.64	8.53	11.21	14.58
$2p_{1/2}$-$2d_{5/2}$	12.84	7.73	5.56	3.61	$1f_{5/2}$-$1g_{9/2}$	8.51	8.22	9.28	10.27
$1f_{5/2}$-$1g_{7/2}$	8.69	7.45	8.57	10.09	$1f_{5/2}$-$1i_{11/2}$	7.93	7.67	10.33	13.71
$1g_{9/2}$-$2f_{7/2}$	8.45	7.29	8.54	10.31	$2p_{3/2}$-$2d_{5/2}$	7.40	7.16	9.34	12.00
$2p_{3/2}$-$2d_{3/2}$	6.98	6.04	7.03	8.38	$2p_{3/2}$-$2d_{3/2}$	7.29	7.06	9.39	12.31
$2d_{5/2}$-$2f_{7/2}$		4.92	11.20	18.60	$1d_{5/2}$-$1h_{11/2}$	5.29	5.09	6.82	9.00
$1d_{5/2}$-$1h_{11/2}$	5.54	4.79	5.60	6.67	$1f_{7/2}$-$2d_{5/2}$	4.31	4.14	5.49	7.17
$1g_{9/2}$-$3p_{3/2}$	5.27	4.57	5.38	6.54	$2p_{3/2}$-$2g_{9/2}$	3.34	3.25	4.39	5.84
$2p_{3/2}$-$2d_{5/2}$	7.28	4.53	3.36	8.39	$2p_{3/2}$-$1g_{7/2}$	3.32	3.22	4.23	5.49

Fig. 11(b), and the angle-integrated inelastic cross sections in Fig. 11(c). The Coulomb interaction was included in the calculations (without any radial cutoff) and is responsible for the plateau in the cross sections for RCUT ≥ 7.5 fm. It is clear from Fig. 11 that the nuclear part of the interaction samples the transition density over a range which extends from about 4–4.5 fm out to about 7.5 fm, although over 75% of the cross section arises from the region $7 \geq r \geq 5$ fm. (We note that the transition density peaks at $r \approx 5.1$ fm.) This is similar to what was found by Bernstein [2] for low-energy alpha-particle scattering, and Satchler [35] for $\pi^{\pm}$ scattering in the vicinity of the (3,3) resonances. This result implies that the interaction is neither sharply localized, nor confined to the extreme tail of the transition density for these "surface"-type reactions. However, as can be seen from Fig. 11(b), the interaction occurs in the tail region of the transition potential in the vicinity of $11 \geq r \geq 7.5$ fm (the strong absorption radius is ~ 9.2 fm). Of course, the extent of the interaction region is expected to be somewhat dependent upon the projectile wavelength (~ 1.5 fm in our case) and the form of the imaginary potential.

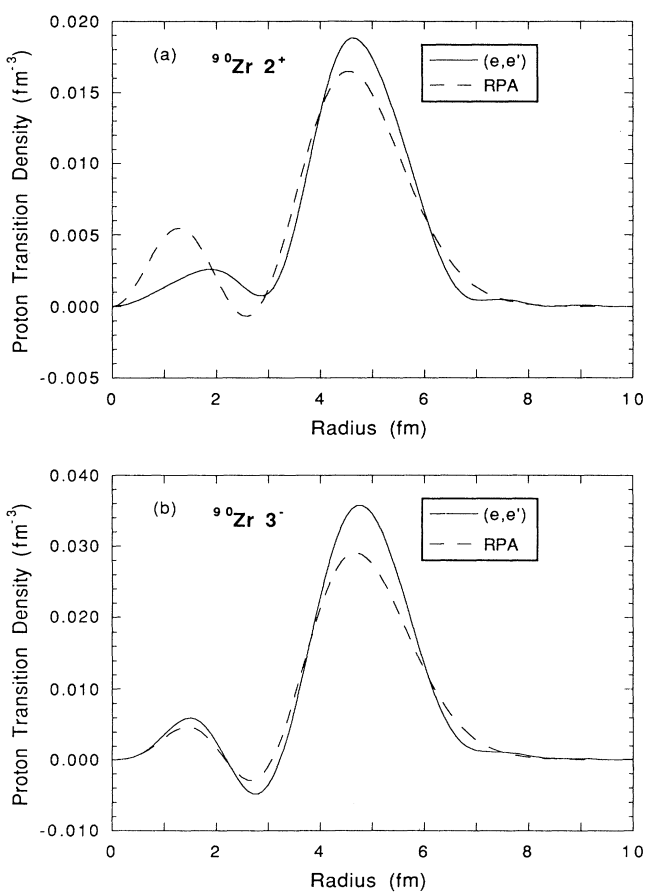

FIG. 8. Comparison of proton transition densities deduced from inelastic electron scattering and RPA calculations for the 2_1^+ and 3_1^- states of ^{90}Zr.

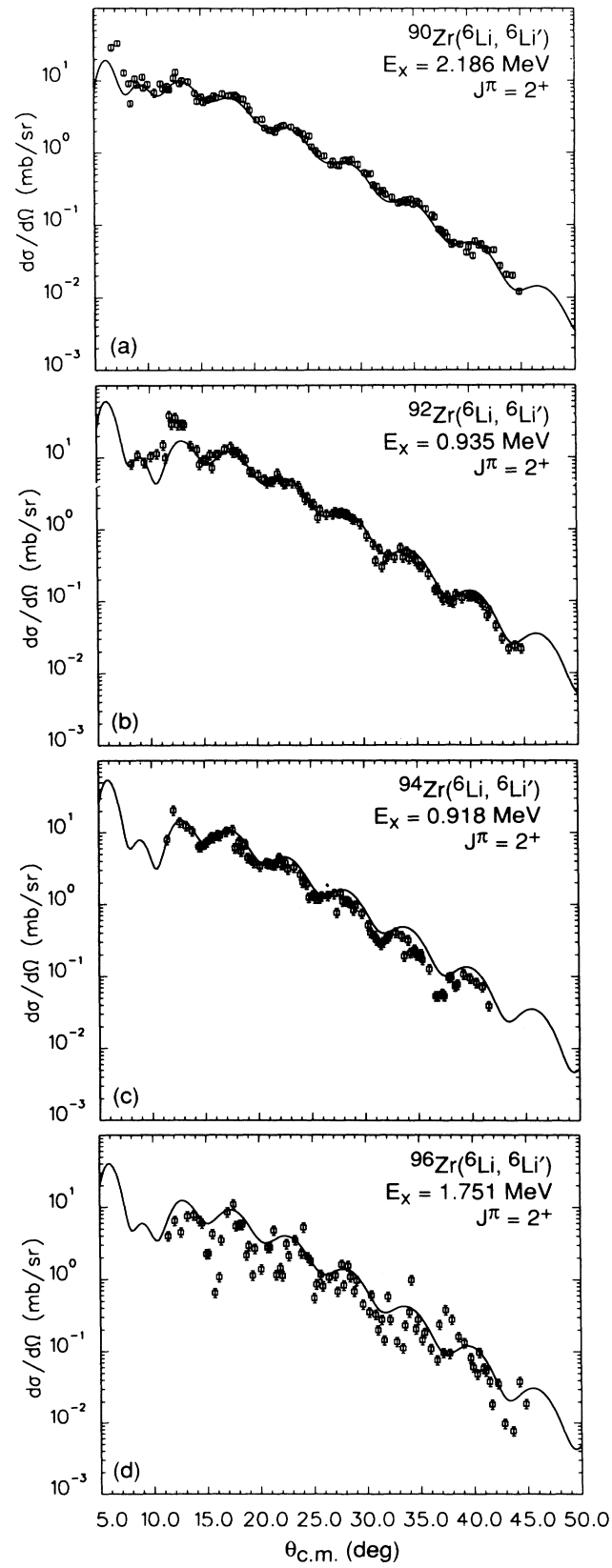

FIG. 9. Comparisons of folding model predictions of the cross sections for exciting the 2_1^+ states of ^{90,92,94,96}Zr by 70-MeV ^{6}Li ions with the experimental data.

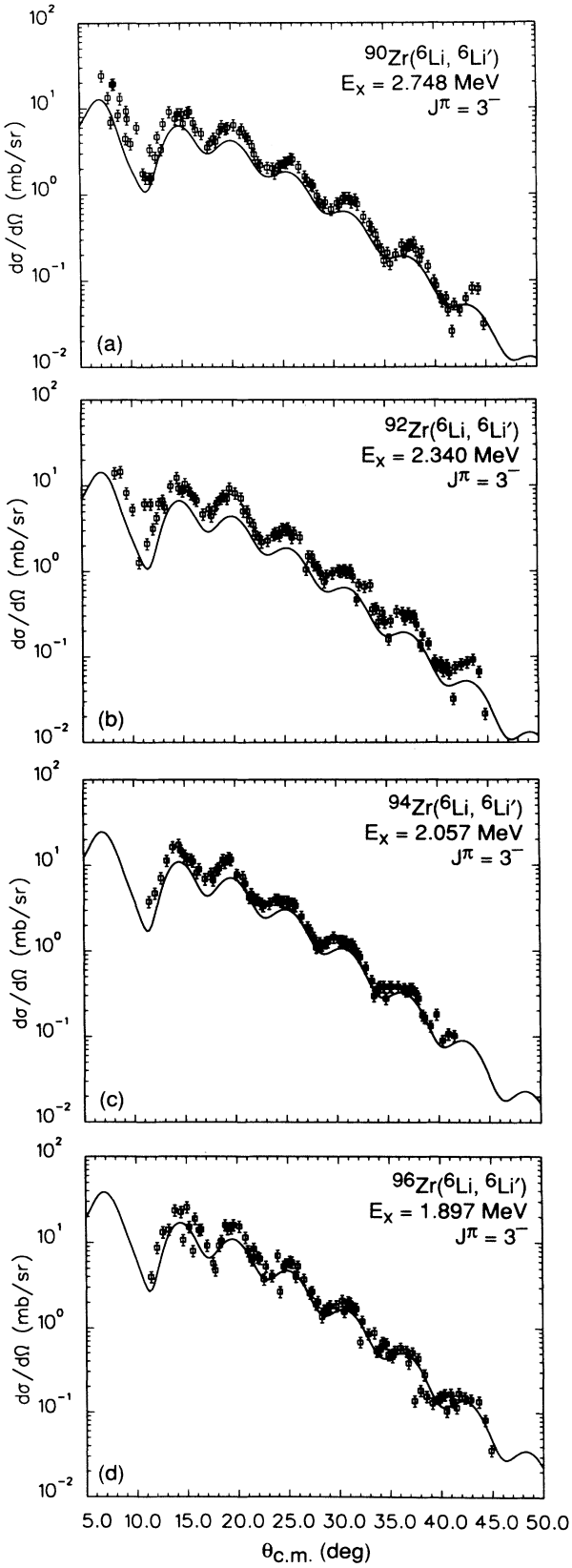

FIG. 10. Comparisons of the folding model predictions of cross sections for exciting the 3_1^- states of ^{90,92,94,96}Zr by 70-MeV ^{6}Li ions with the experimental data.

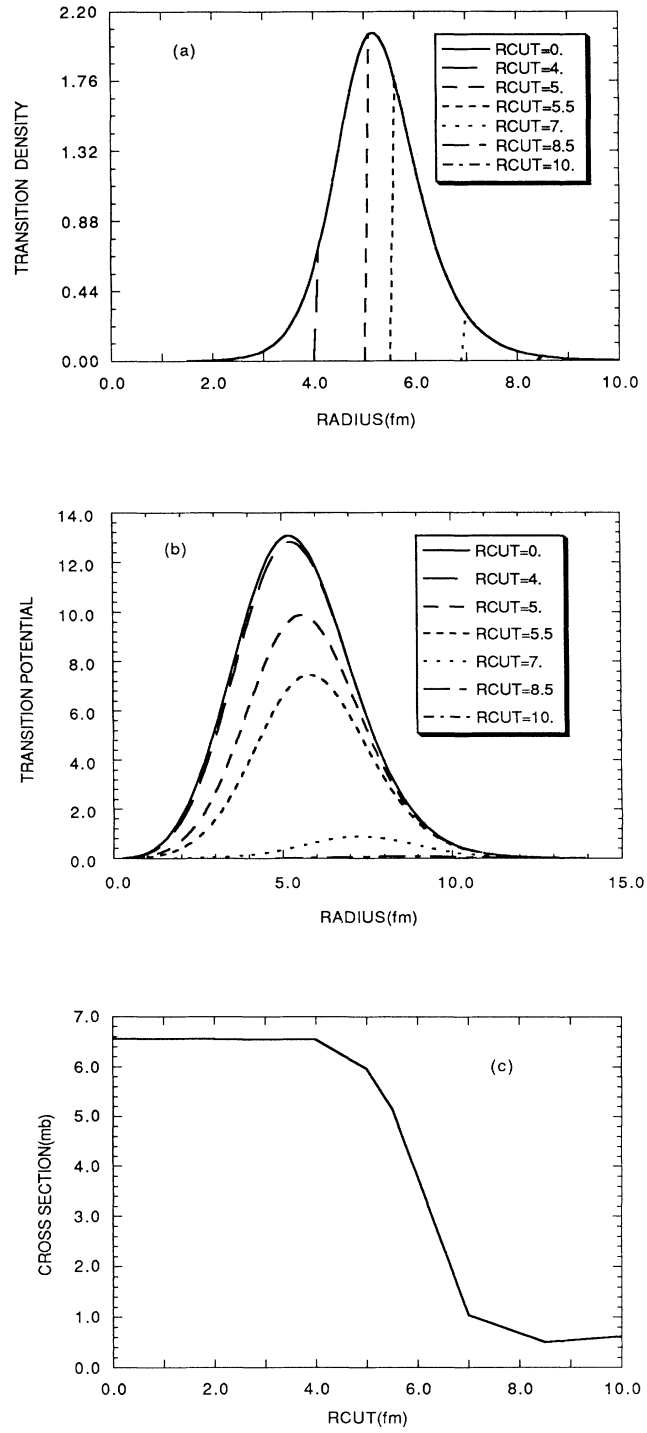

FIG. 11. The effects of a radial cutoff on the 3_1^- excitation in ^{94}Zr. The folding model with our effective nucleon-nucleon interaction and a Tassie transition density was used. (a) Transition density as a function of radius with several radial cuts (RCUT). (b) Transition potentials as a function of radius corresponding to the cutoff transition densities shown in (a). (c) Calculated total inelastic cross sections as a function of RCUT. The calculations include contributions from both nuclear and Coulomb interactions; the asymptotic value of the cross section is due to the Coulomb excitation alone.

IV. COMPARISON WITH PREVIOUS RESULTS

A. Are the reported M_n/M_p consistent?

Also listed in Table III are the M_n/M_p reported by Rychel *et al.* [13] and those by Wang and Rapaport [14], as well as values determined from the RPA calculations. It is clear that the M_n/M_p ratios reported by Rychel *et al.* [13] are considerably larger than both those of Wang and Rapaport [14] and our values. For the 2_1^+ states, our M_n/M_p are in reasonable agreement with those of Wang and Rapaport [14], while our M_n/M_p for the 3^- states are lower for ^{92,94}Zr. In Fig. 12, we compare our deduced M_n/M_p values with those from Wang and Rapaport and the RPA calculations for the 2_1^+ and 3_1^- excitations. Except for ^{90}Zr, the values reported by Rychel *et al.* [13] would lie above the ranges shown in Fig. 12 by large amounts.

It is advisable when comparing M_n/M_p values deduced from different inelastic-scattering measurements to include comparisons of the $B(El)\uparrow$ used in, or implied by, the analyses. Wang and Rapaport [14] do not list the $B(El)\uparrow$ that could be deduced from their comparison of (p,p') and (n,n') data. We have used the $\delta_l^{nn'}$ and $\delta_l^{pp'}$ from the tables in their papers [14] to calculate $B(El)\uparrow$ and to deduce M_n/M_p ratios. To do this, we used the expressions

$$\delta_l^{pp'}(v_{pn}N+v_{pp}Z)=v_{pn}N\delta_l^n+v_{pp}Z\delta_l^p$$

and (13)

$$\delta_l^{nn'}(v_{nn}N+v_{np}Z)=v_{nn}N\delta_l^n+v_{np}Z\delta_l^p\ ,$$

where v_{pn}, e.g., is the interaction between a projectile proton and a target neutron. As with the interaction in our RPA calculations, we assume that the ratio [4] of the unlike interaction $(v_{np}=v_{pn})$ to the like interaction $(v_{nn}=v_{pp})$ is 3/1. We used the δ_l^p so obtained to calculate $B(El)\uparrow$ with Eq. (8). We also calculated M_n/M_p using the relation

$$\delta_l^N=\delta_l^p\left[\frac{1+S_N(M_n/M_p)}{1+S_N(N/Z)}\right]\ , \tag{14}$$

where S_N is the ratio of the like to unlike strengths for neutron scattering $(N=nn',\ S_N=\frac{1}{3})$ and the inverse of this ratio for proton scattering $(N=pp',\ S_N=3)$. The values of M_n/M_p that we calculated in this manner were essentially identical to those given by Wang and Rapaport [14]. We calculated $B(El)\uparrow$ for the results of Rychel *et al.* [13] by converting their tabulated values which were given in single-particle units.

We summarize in Table VII $B(El)\uparrow$ and M_n/M_p from the three works. Here it is seen that for the 2_1^+ of ^{90}Zr, all three works give the same $B(E2)\uparrow$, which is essentially the adopted value [20]. The M_n/M_p ratio of Wang and Rapaport [14] and the present work are in excellent agreement, whereas that noted by Rychel *et al.* [13] is considerably larger. For ^{92}Zr, we see that Wang and Rapaport [14] have a larger $B(E2)\uparrow$ and smaller M_n/M_p than ours, while Rychel *et al.* [13] obtain a $B(El)\uparrow$ smaller than either, with M_n/M_p between 2 to 3 times larger. For ^{94}Zr, the $B(E2)\uparrow$ from Wang and Rapaport [14] is about 60% larger than the adopted value, whereas that of Rychel *et al.* [13] is about 25% lower. We believe that this represents either an inconsistency in the data or in the models used to deduce M_n/M_p. For the 3_1^- state in ^{90}Zr, all three studies again give nearly the same $B(E3)\uparrow$. Our M_n/M_p is only two-thirds that of Wang and Rapaport [14], but the Rychel *et al.* [13] value is two to three times larger than either.

At first sight, the discrepancies with Rychel *et al.* [13] are very surprising. However, for ^{90}Zr they provide a clue as to the reason because they tabulate the δ_l^N values in this case. Furthermore, as mentioned, their $B(El)$ values are very close to those that we use. They give $\delta_2^N=0.406$ fm (versus our value of 0.396 fm) and $\delta_3^N=0.806$ fm (versus our value of 0.686 fm). Since both the alpha particle and ^{6}Li are isoscalar probes, one expects the extracted δ_l^N to be essentially identical if the same $B(El)\uparrow$ is used in the analysis of the data. The noted δ_l^N are in accordance with this expectation, and when used in Eq. (9), yield M_n/M_p values in substantial agreement with those deduced in this work. Consequently, the source of the discrepancy with their quoted M_n/M_p values must be the method they used to derive them from

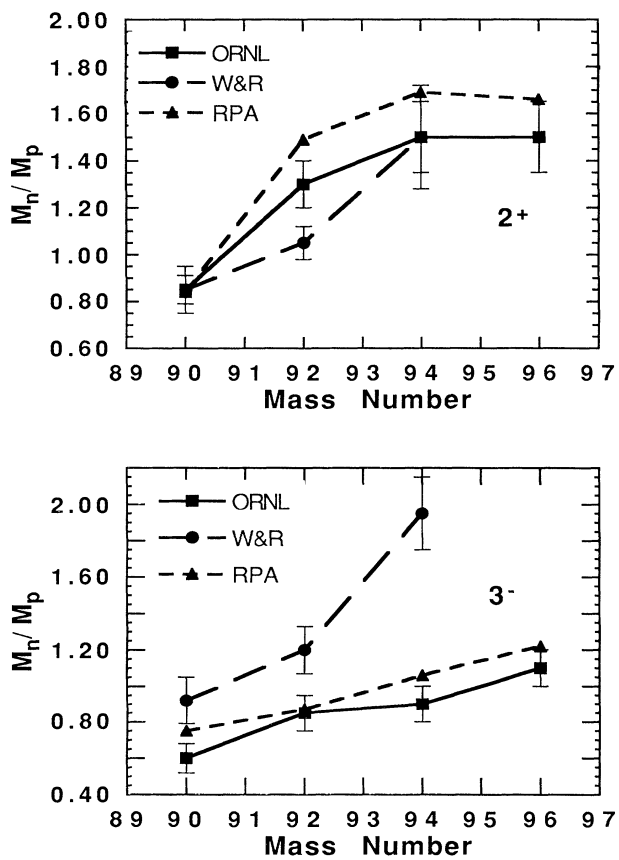

FIG. 12. Comparison of M_n/M_p deduced here (ORNL) for the 2_1^+ and 3_1^- states in ^{90,92,94,96}Zr with predictions from RPA calculations and the values from Ref. [14].

TABLE VII. Summary of $B(El)\uparrow$ and M_n/M_p deduced for 2_1^+ and 3_1^- states in ^{90,92,94,96}Zr.

Nucleus	This work $B(El)\uparrow$[c] ($e^2 b^l$)	This work M_n/M_p	Wang and Rapaport[a] $B(El)\uparrow$[d] ($e^2 b^l$)	Wang and Rapaport[a] M_n/M_p	Rychel *et al.*[b] $B(El)\uparrow$[e] ($e^2 b^l$)	Rychel *et al.*[b] M_n/M_p
2_1^+						
^{90}Zr	0.061	0.85	0.0612	0.85	0.0623	1.22
^{92}Zr	0.083	1.30	0.130	1.05	0.0691	2.91
^{94}Zr	0.066	1.50	0.108	1.50	0.0495	3.02
^{96}Zr	0.055	1.50			0.0274	4.62[g]
3_1^-						
^{90}Zr	0.071	0.60	0.0653	0.92	0.0660	1.80
^{92}Zr	0.067	0.85	0.0634	1.20	0.0556	2.52[h]
^{94}Zr	0.087	0.90	0.0569	1.87[f]	0.0794	2.36
^{96}Zr	0.12	1.10			0.104	2.67

[a]Reference [14].
[b]Reference [13].
[c]Adopted values from Ref. [20] for $B(E2)\uparrow$, and Ref. [25] for $B(E3)\uparrow$ except for ^{96}Zr.
[d]Calculated from δ_l^{ii} values in Ref. [14] with Eq. (12).
[e]Calculated from Table V in Ref. [13].
[f]Authors quote 1.59 which we suspect is a misprint. (See footnotes to Table III.)
[g]Authors quote 4.69 which we suspect is a misprint. (See footnotes to Table III.)
[h]Authors quote 2.17 which we suspect is a misprint. (See footnotes to Table III.)

their deduced δ_l^N and $B(El)$. Their method involves the so-called implicit folding procedure [36], together with corrections for an assumed density dependence of the effective alpha-nucleon interaction [37], rather than the simple relation (9) used here. This is discussed further in the next section.

Although the $B(E3)\uparrow$ of Wang and Rapaport [14] for ^{92}Zr is essentially the same as the adopted value, their M_n/M_p is somewhat larger. For ^{94}Zr, the $B(E3)\uparrow$ of Wang and Rapaport [14] is about 30% smaller than the adopted value, and their M_n/M_p is significantly larger than our value.

B. Partial reanalysis of the alpha-particle data

In view of the apparent large discrepancies with the M_n/M_p reported by Rychel *et al.* [13], we decided to perform a partial reanalysis of those data. To this end, we used the G_{IS} and G_{EM} values listed in their tables as well as the formulas given in their paper to calculate δ_l^N and $B(El)\uparrow$. These were then used in Eqs. (8) and (9) to calculate values of δ_l^p and M_n/M_p ratios. In Table VIII, we compare these values of δ_l^N, $B(El)\uparrow$, and M_n/M_p with those derived from our ^{6}Li data. Since these revised values of M_n/M_p are deduced using the same methods,

TABLE VIII. Comparisons of the δ_l^N and $B(El)\uparrow$ derived from Rychel *et al.* [13] using the tables and formula therein and the M_n/M_p obtained by application of Eq. (9), with the corresponding values derived from our ^{6}Li data.

Nucleus	Rychel *et al.*[a] δ_l^N (fm)	Rychel *et al.*[a] $B(El)\uparrow$ ($e^2 b^l$)	Rychel *et al.*[a] M_n/M_p (DOMP)	(M_n/M_p)[b]	(^{6}Li,^{6}Li′) δ_l^N (fm)	(^{6}Li,^{6}Li′) $B(El)\uparrow$ ($e^2 b^l$)	(^{6}Li,^{6}Li′) M_n/M_p
2_1^+							
^{90}Zr	0.408	0.062±0.006	0.89		0.396	0.063±0.005[c]	0.85
^{92}Zr	0.731	0.069±0.006	2.31	(2.02)	0.557	0.083±0.006[c]	1.30
^{94}Zr	0.633	0.050±0.005	2.48	(2.03)	0.525	0.066±0.014[c]	1.50
^{96}Zr	0.639	0.027±0.007	3.86	(2.43)	0.466	0.055±0.022[c]	1.50
3_1^-							
^{90}Zr	0.806	0.0664	0.94	(0.86)	0.686	0.071	0.60
^{92}Zr	0.894	0.0556	1.44	(1.23)	0.742	0.067	0.85
^{94}Zr	1.020	0.0794	1.53	(1.42)	0.839	0.087	0.90
^{96}Zr	1.228	0.1035	1.77	(1.57)	1.051	0.120	1.10

[a]Calculated by us from contents of Ref. [13].
[b]M_n/M_p of previous column recalculated using $B(El)\uparrow$ from column 7.
[c]From Ref. [20].

they are directly comparable.

As already noted above, the revised M_n/M_p for the 2_1^+ state of ^{90}Zr is in excellent agreement with our value, as well as that of Wang and Rapaport [14]. The revised M_n/M_p for the other states are reduced by about 25–40 % from those tabulated in Ref. [13]. We then recalculate M_n/M_p by using the δ_l^N that we deduce from Rychel *et al.* [13] and $B(El)\uparrow$ adopted for our data. The new values of M_n/M_p are listed within parentheses in column 5 of Table VIII, and it is obvious that the discrepancies with our M_n/M_p are further reduced.

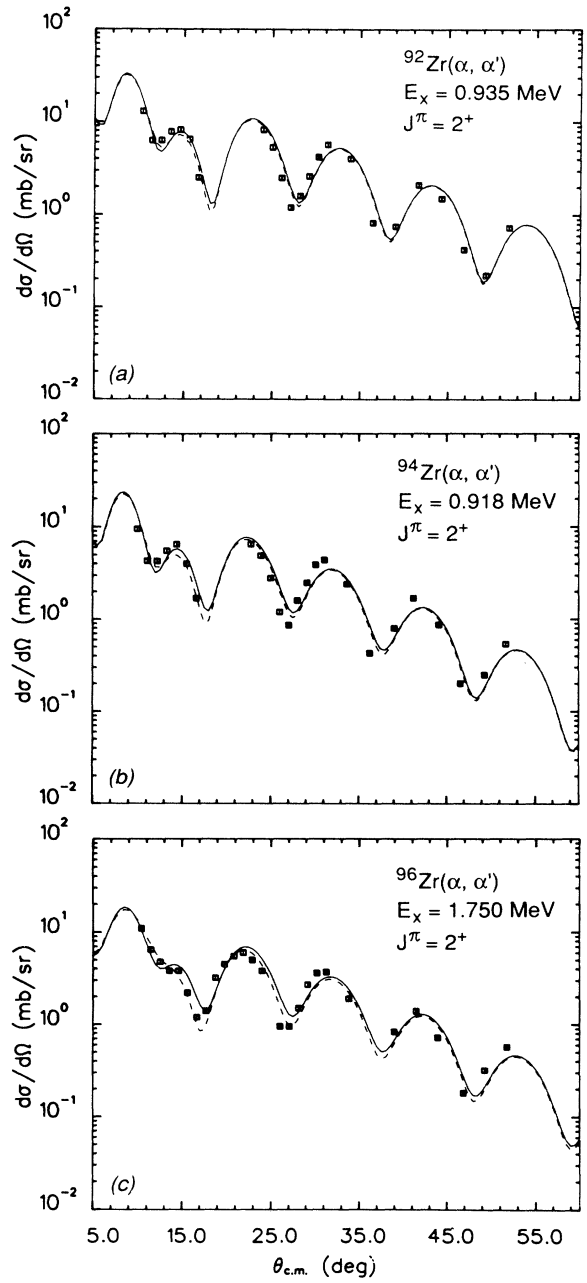

FIG. 13. Comparisons of coupled-channels calculations using the DOMP and the program PTOLEMY with differential cross sections for exciting the 2_1^+ states of ^{92,94,96}Zr by 35.4-MeV alpha particles. The solid curves use δ_l^N that we have calculated from information given in Ref. [13] and our adopted $B(E2)\uparrow$, whereas the dashed curves use the $B(E2)\uparrow$ reported in Ref. [13].

To investigate the validity of this latter procedure, we calculated the inelastic alpha-scattering cross sections using the optical model parameters given in Table 4 of Rychel *et al.* [13] and the δ_l^N given in column 2 and the adopted $B(El)\uparrow$ in column 7 of our Table VIII. The results for exciting the 2_1^+ states of ^{92,94,96}Zr are plotted in Fig. 13 as the solid curves, and compared with the least-squares-fitted curves (dashed) and data from Rychel *et al.* [13]. (As these data are no longer available, we read them from the published figures of Ref. [13]. We estimate the errors in this procedure to be less than a few tenths of a degree in angle, and a few percent in cross section.) No figures are shown for the 2_1^+ state of ^{90}Zr state as the two calculations are indistinguishable. For the 2_1^+ states of ^{92,94}Zr, use of the adopted $B(E2)\uparrow$ for calculating the cross sections (solid curves) appears to fit the data equally well as the least-squares-fitted curves of Rychel *et al.* [13] (dashed), indicating that the uncertainties on the $B(E2)\uparrow$ reported for these two transitions are somewhat optimistic. Use of our adopted $B(E2)\uparrow$ for the 2_1^+ state of ^{96}Zr, which is twice that deduced by Rychel *et al.* [13], does result in a somewhat poorer fit to the alpha data in the Coulomb nuclear interference region near 15°. The 2_1^+ data beyond $\theta_{c.m.} \approx 15°$ for ^{92,94,96}Zr seem to be shifted to smaller angles by $\sim 0.5°$ compared to the theoretical predictions. Such a shift is not apparent in the inelastic alpha data for the other cases.

It should be noted in Table VIII that, except for the 2_1^+ state of ^{90}Zr, all of the δ_l^N from the alpha scattering are larger than the corresponding δ_l^N from the ^{6}Li scattering, and this accounts for the fact that M_n/M_p in column 5 are still from 35 to 55 % larger than our values. Obviously, if the δ_l^N were reduced to our values and used to calculate the alpha cross sections using the DOMP method, the latter would grossly underestimate the observed cross sections. Hence, although we are able to explain part of the discrepancies between the large values of M_n/M_p as reported in Ref. [13] relative to those of Wang and Rapaport [14] and ourselves, we are not able to completely resolve the problem, at least in the context of the DOMP model.

In addition, we performed folding model calculations

TABLE IX. Strengths of the real and imaginary parts of the effective alpha-nucleon interaction with Gaussian form and a range of 1.94 fm which fit the elastic scattering from the zirconium isotopes.

A	v (MeV)	w (MeV)
90	43.60	12.61
92	45.22	15.66
94	47.46	14.95
96	48.52	15.39

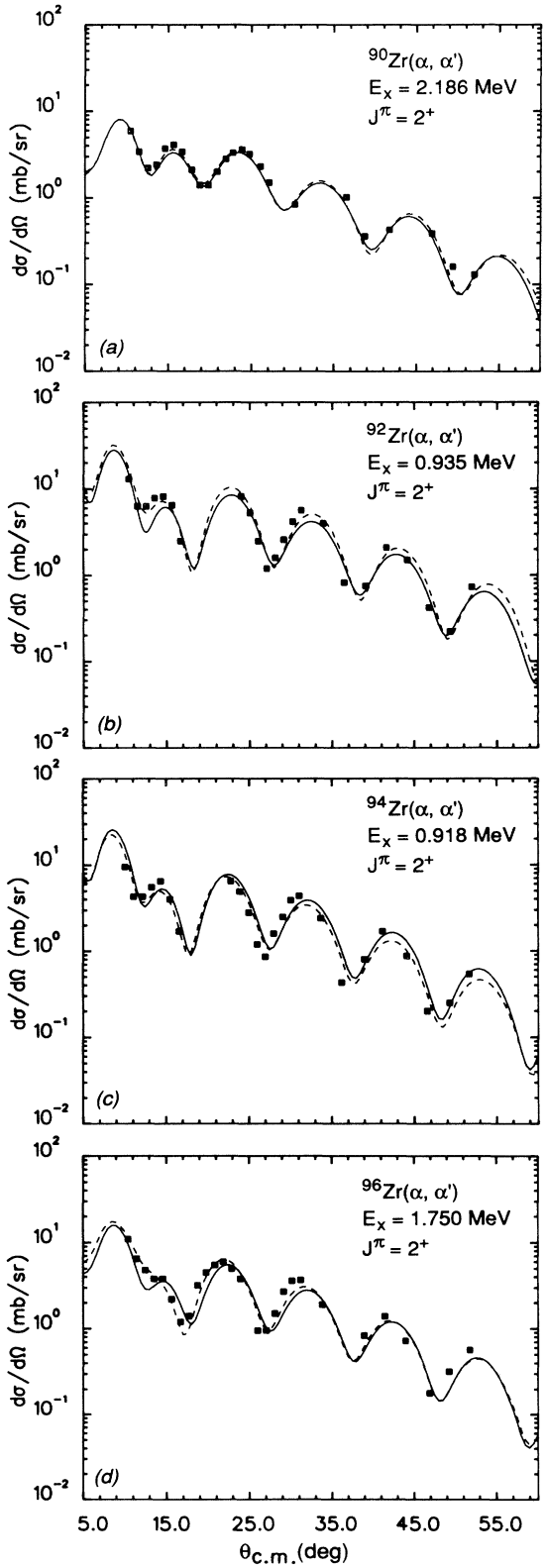

FIG. 14. Comparison of folding model predictions (solid curves) of the cross sections for exciting the 2_1^+ states of ^{90,92,94,96}Zr by 35.4-MeV alpha particles with the experimental data from Ref. [13], and with the DOMP fits of Ref. [13] (dashed curves).

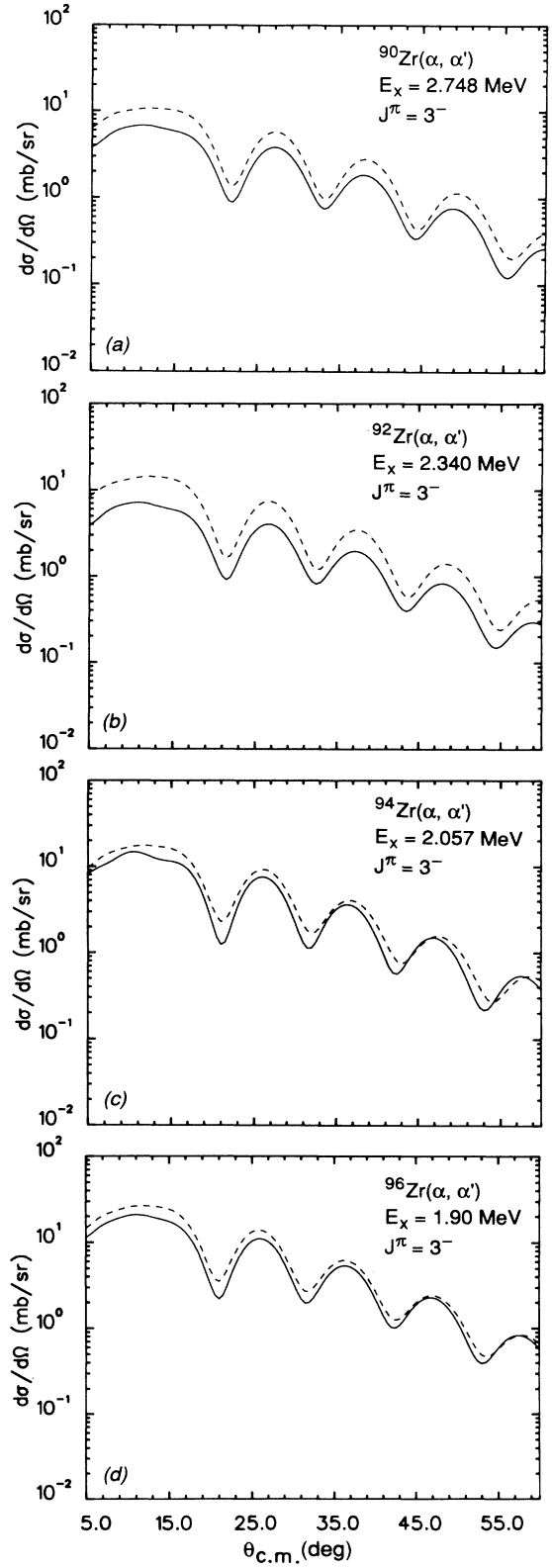

FIG. 15. Comparison of folding model predictions (solid curves) of the cross sections for exciting the 3_1^- states of ^{90,92,94,96}Zr by 35.4-MeV alpha particles with the DOMP fits (dashed curves) from Ref. [13]. (The DOMP fits follow closely the measured cross sections.)

similar to those described earlier for ^{6}Li, but applying a Gaussian form for the effective alpha-nucleon interaction. The range was chosen to be 1.94 fm [38] and the complex strength parameters were obtained from fits to the elastic data [39] (see Table IX). The same RPA transition densities as shown in Figs. 6 and 7 were used. The calculated cross sections (solid curves) are compared with the 2_1^+ data and the DOMP fits (dashed curves) of Rychel *et al.* [13] in Fig. 14. Comparisons of the calculated cross sections (solid curves) with the DOMP fits (dashed curves) of Rychel *et al.* [13], which are essentially equivalent to the data, for the 3_1^- states are shown in Fig. 15. As can be seen from a comparison of these figures with the corresponding figures (i.e., Figs. 9 and 10) for the ^{6}Li data, the agreement between the folding model calculations and the data is of the same quality for both projectiles. Consequently, this more "microscopic" approach implies consistency between the ^{6}Li and alpha-particle measurements, and does not indicate large discrepancies such as were implied by the analyses using the DOMP model.

C. Effects of valence neutrons on isospin character

The trends in the values of M_n/M_p indicate that the effect of the valence neutrons in driving this ratio toward (and larger than) N/Z is much weaker for the 3^- states than for the 2^+ states. Because of strong polarization effects, the differences in this behavior cannot be inferred easily from simple shell-model arguments. However, some physical insight can be obtained by expressing the ratio M_n/M_p in terms of the calculated "valence" (M_i^v) and "core" (M_i^c) contributions to the moments, i.e.,

$$M_n/M_p=(M_n^c/M_p^c)(1+M_n^v/M_n^c)/(1+M_p^v/M_p^c) \quad (15)$$

From the RPA calculations, the ratios of the core contributions, M_n^c/M_p^c, are found to be nearly the same for the quadrupole and octupole transitions considered here, and to have values close to N/Z. Because the valence protons occupy the fp orbits where the valence particle-hole $E2$ transition densities are small and the only recoupling contribution can arise from $g_{9/2}$ orbitals which are sparsely populated, M_p^v is small and relatively independent of the neutron number. On the other hand, the neutron valence contribution is changing rapidly from $M_n^v=0$ in ^{90}Zr which has a closed $N=50$ shell, to values of $M_n^v>M_p^v$ for ^{92,94,96}Zr where several two-quasiparticle states can contribute to the 2^+ excitation. The major neutron 2^+ valence contributions arise from the $2d_{5/2}^2$ recoupling and the $2d_{5/2}$-$3s_{1/2}$ transitions (see Table VI). The magnitude of the $2d_{5/2}^2$ matrix element is nearly the same for ^{92}Zr and ^{94}Zr which have similar neutron configurations (i.e., $2d_{5/2}^2$ and $2d_{5/2}^{-2}$, respectively). This component decreases for ^{96}Zr because of the approximate filling of the $2d_{5/2}$ orbit. The increasing contribution from the $3s_{1/2}$-$2d_{5/2}^{-1}$ p-h transition from ^{92}Zr to ^{96}Zr results in a larger ratio of M_n/M_p for ^{94}Zr relative to ^{92}Zr, but is not sufficient to overcome the decreased contribution from recoupling in the $2d_{5/2}$ orbit in going from ^{94}Zr to ^{96}Zr.

The situation for the 3^- transitions is completely different. Here the valence proton p-h transitions (dominated by $g_{9/2}$-$p_{3/2}^{-1}$) are quite strong and the $p_{3/2}$,$f_{5/2}$ orbits are full. Although the neutron p-h transition $h_{11/2}$-$d_{5/2}^{-1}$ is reasonably strong, there are only two particles in the $d_{5/2}$ orbit at ^{92}Zr. Hence, the factor multiplying M_n^c/M_p^c in Eq. (15) is considerably less than 1 for ^{92}Zr. Although the magnitude of M_n^v increases proportionally with the number of added neutrons, the increase in the ratio M_n^v/M_n^c is somewhat moderated because M_n^c is also increased. The net effect is to drive M_n/M_p upward toward N/Z, but at a rate much reduced compared to that for the 2_1^+ transitions.

The results of the RPA calculations are compared with the data in Table III and in Fig. 12. As shown in Fig. 12, both the trends and magnitudes of the RPA values are similar to those exhibited by the M_n/M_p determined in this work.

V. CONCLUSIONS

We have measured cross sections for the scattering of 70-MeV ^{6}Li ions by ^{90,92,94,96}Zr, and analyzed the data by means of two methods: (1) A macroscopic model in which we fit the elastic data using an optical potential of Woods-Saxon form, and apply the deformed generalization of this (DOMP) to analyze the inelastic data. (2) A microscopic model which uses an effective nucleon-nucleon interaction with a Yukawa form factor and a folding calculation with strengths obtained by fitting the elastic data; this interaction is then folded with transition densities from RPA calculations to predict inelastic cross sections.

In the macroscopic calculations, we have fixed the $B(El)\uparrow$ using adopted values (when known), and deduced nuclear deformation lengths from comparisons of the calculated and measured cross sections. These were then used to derive M_n/M_p ratios using the schematic relation (9). For the excitation of the 2_1^+ states in ^{90,92}Zr, we were also able to search on the data allowing both the potential deformation length δ_l^N and $B(El)\uparrow$ to vary simultaneously. The $B(El)\uparrow$ that we obtained from these fits agreed well with the adopted values. In the RPA calculations, the interaction strengths were determined to reproduce the $B(El)\uparrow$ values used in the macroscopic analyses. We then find good agreement between the ratios of M_n/M_p predicted by the RPA calculations and the values deduced from our data. Our values of M_n/M_p are considerably smaller than those reported by Rychel *et al.* [13] and in much better agreement with those of Wang and Rapaport [14]. However, for the 3_1^- states, our M_n/M_p are smaller than those of Wang and Rapaport [14], and also are less than N/Z for all four isotopes. We have discussed some reasons for these differences. In particular, a considerable portion of the discrepancies with the M_n/M_p ratios reported by Rychel *et al.* [13] arise in part from their use of different $B(El)$ values, and in part from the different procedure used to relate their δ_l^N and $B(El)$ to M_n/M_p.

The fact that δ_l^N deduced by Rychel *et al.* [13] for the 2_1^+ and 3_1^- states of ^{90}Zr are in excellent agreement with

those deduced in this work, while all the other δ_l^N are considerably higher than ours, remains a puzzle. This is compounded by the good reproduction of the 2_1^+ cross sections for both sets of data using the same RPA transition densities in folding calculations. This might suggest an inconsistency in the interpretation of the δ_l^N extracted from the two sets of data using the DOMP for ^{92,94,96}Zr, or possibly an inconsistency in the data themselves.

It is clear from this study that the extraction of M_n/M_p values by studying Coulomb and nuclear interference with low-energy projectiles requires very accurate data, and preferably independent determinations of $B(El)\uparrow$, especially for the 3_1^- excitations. The lack of precise $B(El)\uparrow$ values for the analysis of such data has already been noted by Satchler [39] in an earlier reanalysis of the data of Rychel *et al.* [13].

We note that our data for the 3_1^- state of ^{96}Zr would suggest a very small M_n/M_p ratio (<0.5) if we adopt the recently reported [26,27] large $B(E3)\uparrow$ ($\approx 0.25\ e^2 b^3$) in our DOMP calculations. If this large $B(E3)\uparrow$ is correct, it would imply that the DOMP may not be a valid prescription for deducing M_n/M_p from our data for this transition. Clearly, further experimental effort to settle this question is very desirable.

The RPA transition densities, after folding with the effective interaction determined by fitting the elastic data, predict cross sections in quite good agreement with the measured ones for the 2_1^+ states, but underestimate the cross sections for exciting the 3_1^- states by amounts ranging from about 20% for ^{96}Zr to almost a factor of 2 for ^{92}Zr. At this juncture, it is not clear to what extent the agreement for the 2_1^+ cross sections is a confirmation that both the effective nucleon-nucleon interaction and calculated transition densities are meaningful, or whether these results are fortuitous in light of the calculations for the 3_1^- states.

One possibility is that the Yukawa interaction, whose monopole part was determined by the elastic data, is inappropriate for higher multipoles. A first step in exploring this question was taken by substituting a Gaussian form and following the same procedures. However, the 2_1^+ and 3_1^- cross sections obtained were almost identical to those found using the Yukawa form. This question will be explored further elsewhere [30].

ACKNOWLEDGMENTS

We would like to thank Dr. J. Heisenberg for sending us the results of his most recent analysis of the (e,e') data for the 3_1^- state in ^{90}Zr, and Dr. L. Ray for transmitting the proton transition densities for the ^{90}Zr states. This research was sponsored by the U.S. Department of Energy under Contract No. DE-AC05-84OR21400 with Martin Marietta Energy Systems, Inc., No. W-7405-ENG-48 at Lawrence Livermore National Laboratory, Grant Nos. DE-FG06-86ER40283 at Oregon State University, and DE-FG02-91ER-40609 at Yale University. One of us (V.A.M.) would like to acknowledge the Oak Ridge National Laboratory and the Joint Institute for Heavy Ion Research for providing partial support during phases of this work.

[1] G. R. Satchler, *Direct Nuclear Reactions* (Oxford University Press, New York, 1983); Nucl. Phys. **A472**, 215 (1987).
[2] A. M. Bernstein, Adv. Nucl. Phys. **3**, 325 (1969).
[3] V. A. Madsen, V. R. Brown, and J. D. Anderson, Phys. Rev. Lett. **34**, 1398 (1975); Phys. Rev. C **12**, 1205 (1975).
[4] A. M. Bernstein, V. R. Brown, and V. A. Madsen, Phys. Lett. **103B**, 255 (1981); **106B**, 259 (1981).
[5] V. R. Brown and V. A. Madsen, Phys. Rev. C **11**, 1298 (1975); **17**, 1943 (1978).
[6] D. J. Horen, J. R. Beene, and F. E. Bertrand, Phys. Rev. C **37**, 888 (1988).
[7] J. R. Beene, F. E. Bertrand, D. J. Horen, R. L. Auble, B. L. Burks, J. Gomez del Campo, M. L. Halbert, R. O. Sayer, W. Mittig, Y. Schutz, J. Barrette, N. Alamanos, F. Auger, B. Fernandez, A. Gillibert, B. Haas, and J. P. Vivien, Phys. Rev. C **41**, 920 (1990).
[8] D. J. Horen, F. E. Bertrand, J. R. Beene, G. R. Satchler, W. Mittig, A. C. C. Villari, Y. Schutz, Zhen Wenlong, E. Plagnol, and A. Gillibert, Phys. Rev. C **42**, 2412 (1990); **44**, 2385 (1991).
[9] D. J. Horen, R. L. Auble, J. R. Beene, F. E. Bertrand, M. L. Halbert, G. R. Satchler, M. Thoennessen, R. L. Varner, V. R. Brown, P. L. Anthony, and V. A. Madsen, Phys. Rev. C **44**, 128 (1991).
[10] S. J. Seestrom-Morris, C. L. Morris, J. M. Moss, T. A. Carey, D. Drake, J. C. Douse, and G. S. Adams, Phys. Rev. C **33**, 1847 (1986).
[11] J. L. Ullmann, P. W. F. Alons, B. L. Clausen, J. J. Kraushaar, J. H. Mitchell, R. J. Peterson, R. A. Ristinen, R. L. Boudrie, N. S. P. King, C. L. Morris, J. N. Knudson, and E. F. Gibson, Phys. Rev. C **35**, 1099 (1987).
[12] D. J. Horen, C. L. Morris, S. J. Seestrom, F. W. Hersman, J. R. Calarco, M. Holtrop, M. Leuschner, Mohini J. Rawool-Sullivan, R. W. Garnett, S. J. Greene, M. A. Plum, and J. D. Zumbro, Phys. Rev. C **46**, 499 (1992).
[13] D. Rychel, R. Gyufko, B. van Krüchten, M. Lahanas, P. Singh, and C. A. Wiedner, Z. Phys. A **326**, 455 (1987).
[14] Y. Wang and J. Rapaport, Nucl. Phys. **A517**, 301 (1990); Z. Phys. A **331**, 305 (1988).
[15] G. R. Satchler, unpublished.
[16] V. R. Brown, J. A. Carr, V. A. Madsen, and F. Petrovich, Phys. Rev. C **37**, 1537 (1988).
[17] D. Shapira, G. L. Bomar, J. L. C. Ford, Jr., J. Gomez del Campo, and L. C. Dennis, Nucl. Instrum. Methods **169**, 77 (1980).
[18] M. H. Macfarlane and S. C. Pieper, Argonne National Laboratory Report ANL-76-11, 1978 (unpublished); M. Rhoades-Brown, M. H. Macfarlane, and S. C. Pieper, Phys. Rev. C **21**, 2417 (1980); **21**, 2436 (1980).
[19] Y. P. Gangrskii and I. K. Lemberg, Yad. Fiz. **1**, 1025 (1956) [Sov. J. Nucl. Phys. **1**, 731 (1965)].
[20] S. Raman, C. H. Malarkey, W. T. Milner, C. W. Nestor, and P. Stelson, At. Data Nucl. Data Tables **36**, 1 (1987).
[21] L. N. Galperin, A. Z. Ilyasov, I. K. Lemberg, and G. A. Firsonov, Yad. Fiz. **9**, 225 (1969) [Sov. J. Nucl. Phys. **9**, 133 (1969)].

[22] D. K. Alkhazov, D. S. Andreev, V. D. Vasilov, Y. P. Gangrskii, and I. K. Lembrg, Y. I. Udralov, Izv. Akad. Nauk, USSR, Ser. Fiz. **27**, 1285 (1963) [Bull. Acad. Sci. USSR, Phys. Ser. **27**, 1263 (1964)].
[23] J. Raynal, Phys. Rev. C **23**, 2571 (1981); ECIS88, private communication.
[24] J. Heisenberg, private communication.
[25] R. H. Spear, At. Data Nucl. Data Tables **42**, 55 (1989).
[26] H. Mach, S. Çwiok, W. Nazarewicz, B. Fogelberg, M. Moszynski, J. Winger, and R. L. Gill, Phys. Rev. C **42**, R811 (1990).
[27] H. Ohm, M. Liang, G. Molnar, S. Raman, K. Sistemich, and W. Unkelbach, Phys. Lett. B **241**, 472 (1990).
[28] G. R. Satchler and W. G. Love, Phys. Rep. **55**, 183 (1979).
[29] I. Angeli, M. Beiner, R. J. Lombard, and D. Mas, J. Phys. G **6**, 303 (1980).
[30] G. R. Satchler, D. J. Horen, V. A. Madsen, V. R. Brown, and P. L. Anthony, unpublished.
[31] L. S. Kisslinger and R. A. Sorenson, Rev. Mod. Phys. **35**, 853 (1963).
[32] A. Graue, L. H. Herlanol, K. J. Lervik, J. T. Nesse, and E. R. Cosman, Nucl. Phys. **A187**, 141 (1972); C. R. Bingham and M. L. Halbert, Phys. Rev. C **2**, 2297 (1970).
[33] O. Schwentker, J. Dawson, J. Robb, J. Heisenberg, J. Lichtenstadt, C. N. Papanicolas, J. Wise, J. S. McCarthy, L. T. van der Bijl, and H. P. Blok, Phys. Rev. Lett. **50**, 15 (1983); J. Heisenberg, private communication.
[34] M. L. Barlett, G. W. Hoffman, and L. Ray, Phys. Rev. C **35**, 2185 (1987), and references cited therein.
[35] G. R. Satchler, ORNL Report ORNL-6689, 1991, p. 187.
[36] G. J. Wagner, P. Grabmayr, and H. R. Schmidt, Phys. Lett. **113B**, 447 (1982).
[37] D. K. Srivastava and H. Rebel, Z. Phys. A **316**, 225 (1984).
[38] G. R. Satchler, Nucl. Phys. **A491**, 413 (1989).
[39] P. Singh, S. Kailas, and A. Navin, Z. Phys. A **331**, 309 (1988); P. Singh, private communication.